Annu. Rev. Astron. Astrophys. 2001. 39:403–55

HERBIG-HARO FLOWS: Probes of Early Stellar Evolution

Bo Reipurth and John Bally
Center for Astrophysics and Space Astronomy, University of Colorado, Boulder, Colorado 80309; e-mail: reipurth@casa.colorado.edu, bally@casa.colorado.edu

Key Words Herbig-Haro objects, jets and outflows, star formation

■ **Abstract** Outflow activity is associated with all stages of early stellar evolution, from deeply embedded protostellar objects to visible young stars. Herbig-Haro (HH) objects are the optical manifestations of this powerful mass loss. Analysis of HH flows, and in particular of the subset of highly collimated HH jets, provides indirect but important insights into the nature of the accretion and mass-loss processes that govern the formation of stars. The recent recognition that HH flows may attain parsec-scale dimensions opens up the possibility of partially reconstructing the mass-ejection history of the newly born driving sources and, therefore, their mass-accretion history. Furthermore, HH flows are astrophysical laboratories for the analysis of shock structures, of hydrodynamics in collimated flows, and of their interaction with the surrounding environment. HH flows may be an important source of turbulence in molecular clouds. Recent technological developments have enabled detailed observations of outflows from young stars at near-infrared, mid-infrared, submillimeter, millimeter, and centimeter wavelengths, providing a comprehensive picture of the outflow phenomenon of young stars.

1. INTRODUCTION

Herbig-Haro (HH) objects are small nebulae with characteristic emission line optical spectra found in star-forming regions and which are now recognized as manifestations of outflow activity from newborn stars. The discovery of HH objects dates back half a century to the pioneering papers by Herbig (1950, 1951) and Haro (1952, 1953). The early development of the field was discussed in an earlier review (Schwartz 1983a), as well as in the first symposium devoted to HH objects (e.g., Böhm 1983). In this review, we focus on the subsequent major observational developments that have taken place in the past 18 years. Perhaps the key advancement in our understanding of the subject was the recognition that HH objects are parts of bipolar outflows from very young stars and may take the form of highly collimated jets (e.g., Dopita et al. 1982b, Mundt & Fried 1983, Graham & Elias 1983, Mundt et al. 1984, Reipurth et al. 1986, Mundt et al. 1987).

Jets and outflows have also been recognized in many other fields of astronomy and are associated with objects as diverse as protoplanetary nebulae, massive and low-mass X-ray binaries, symbiotic systems, black hole X-ray transients, and active galactic nuclei. As a result, today we see the jet phenomenon as a universal process in the evolution of many classes of astrophysical objects (e.g., Livio 1999). To the extent that the fundamental underlying physical principles may be the same for all these objects, the study of HH jets has consequences that reach far beyond the realm of newborn stars.

Initially very rare objects, HH flows—thanks to modern widefield imagers—are now commonly found in star-forming regions. In the latest census, about 600 HH objects were catalogued (Reipurth 2001).

A number of reviews of various aspects of HH flows and associated outflow phenomena from young stars have appeared recently, including those of Bachiller (1996), Rodríguez (1997), Reipurth & Raga (1999), Hartigan et al. (2000a), and Eislöffel et al. (2000a). So far, the most complete exposition of HH research was presented at the second symposium on HH objects held in Chamonix, France, in 1997 (Reipurth & Bertout 1997).

2. MORPHOLOGY OF HH FLOWS

HH objects are generally small (20–30 arcsec) nebulae with a nondescript or chaotic shape, often found in pairs or in strings of objects. Some HH objects have bow shapes and others have an obvious jet-like morphology. But although the most commonly depicted images of HH objects show a well-collimated jet ending in a bright symmetric bow shock, such fine morphologies are rare. Examples of well-developed jet and bow shock systems are shown in Figures 1 and 2. It is well established that HH objects are shocks in bipolar outflows from newborn stars, but individual environments, the chaotic nature of shocks, varying evolutionary stages, and differing extinction all act to produce a rich, even bewildering, array of morphologies (Figure 3).

2.1. The Detailed Structure of Working Surfaces

The most violent action in a protostellar outflow occurs at the "terminal working surface" where the supersonic flow slams directly into the undisturbed ambient medium. Somewhat milder collisions can occur within outflows whose ejection velocity varies with time. An "internal working surface" can form where faster-moving gas catches up with and "rear-ends" slower-moving material ejected earlier (Raga et al. 1990). In either case, a two-shock structure results, consisting of a "reverse shock," which decelerates the supersonic flow, and a "forward shock," which accelerates the material with which it collides (e.g., Hartigan 1989). The forward shock may take the form of a bow shock whose surface is normal to the flow direction on axis, but which becomes increasingly oblique away from the

axis in the swept-back wings. A succession of increasingly sophisticated models of working surfaces has been developed and compared with the observed characteristics of HH objects of this type: The earliest "1.5 dimensional models," in which the emission from an idealized bow shock is synthesized as the superposition of oblique plane shocks (e.g., Hartmann & Raymond 1984, Raga & Böhm 1985, 1986, Hartigan et al. 1987) have been followed by full two- and three-dimensional hydrodynamic simulations of bow shocks (e.g., Raga & Böhm 1987, Raga et al. 1988) and complete working surfaces (e.g., Blondin et al. 1989, Stone & Norman 1993, de Gouveia Dal Pino & Benz 1993).

Radiative shocks consist of a very thin layer at the shock front, where gas is heated and ionized, followed by a much more extended "cooling zone" (e.g., Ostriker & McKee 1988). Most of the radiation from the shock arises in the cooling zone, where the gas emits forbidden lines of metals and recombination lines of hydrogen. If the preshock material is partially neutral, hydrogen atoms entering the shock will be excited by collisions before being ionized, giving rise to strong Balmer line emission from the shock front itself (Chevalier & Raymond 1978, Heathcote et al. 1996). However, if the shock velocity exceeds $\sim$110 km s^{-1}, the ionizing flux emitted by the shock will completely ionize the preshock material (Cox & Raymond 1985). The cooling and recombination of the postshock gas results in stratification such that lines from species of successively lower excitation dominate the emission at greater and greater distances behind the shock front. Consequently, the brightness of high-excitation lines such as [OIII] should peak closer to the shock front than low-excitation lines such as [SII]. For typical parameters, the thickness of the cooling zone ($d \sim 5 \times 10^{14} n_{100}^{-1} V_{100}^{4}$ cm, where n_{100} is the density in units of 100 cm^{-3} and V_{100} is the shock speed in units of 100 km s^{-1}) is often too small to be resolved in ground-based images so that only the integrated properties of the shock may be studied. However, the stratification of the cooling zone often can be observed at the resolution of the Hubble Space Telescope (HST).

To date, the WFPC2 imager onboard HST has been used to obtain narrow-band images of 10 working surfaces: HH 1 and HH 2 (Schwartz et al. 1993, Hester et al. 1998), HH 29 (Devine et al. 2000a), HH 32 (Curiel et al. 1997), HH 34 (Ray et al. 1996), HH 47A and HH 47D (Heathcote et al. 1996), HH 80 and HH 81 (Heathcote et al. 1998), and HH 111V (Reipurth et al. 1997b).

Of these objects, HH 34 perhaps resembles best the idealized bow-shock models. Figure 4 shows a composite of WFPC2 Hα and [SII] images of HH 34. The approximately parabolic outline of HH 34 is delineated by intricate, narrow (in some cases unresolved) Hα filaments. Broader bands of very faint [SII] emission run parallel to these Balmer filaments along their inside edge, especially in the oblique wings of HH 34. The Hα bright filaments result from collisional ionization of hydrogen at the shock front while the trailing [SII] emission comes from the postshock cooling zone. Thus, the *HST* images dramatically illustrate that the cooling zone behind the forward shock in HH 34 is quite extended, a result already suggested by ground-based data (Bührke et al. 1988, Morse et al. 1992) and analyzed theoretically by Raga & Binette (1991). The thin skin of collisionally

excited Hα wraps around the apex of the bow shock and appears as a bright rim where the line of sight runs tangent to its surface. Similarly, the Hα filaments seen in the interior of HH 34 probably arise where corrugations in the surface of the shock front cause it to lie along the line of sight (some diffuse Hα emission may also be produced by recombination in the postshock gas). A similar structure of Balmer filaments enveloping clumps of [SII] bright material is also seen in HH 1 (Hester et al. 1998) and HH 111V (Reipurth et al. 1997b).

A straightforward prediction of bow-shock models is that the shock strength should be greatest at the apex of the bow, where the shock is normal, and should decline in the wings, where the shocks become increasingly oblique. This is indeed observed in the most symmetric bow shocks, where high-excitation lines dominate around the apex and lower-excitation lines are strong along the wings.

2.2. Jets

The recognition that some HH objects take the form of highly collimated "jets" (e.g., Dopita et al. 1982b, Mundt & Fried 1983) was central to the development of our current concept of HH objects as the visible manifestations of collimated outflows from young stars. Subsequently, considerable observational and theoretical effort has been focused on elucidating the properties and origins of such jets. In ground-based images, HH jets typically appear as linear or gently wiggling chains of compact knots, sometimes connected by fainter emission, and having length-to-width ratios of 10:1 or more. In many cases, these jets point toward more extended bow-shaped HH objects, as discussed in the previous section.

From the moment of their recognition, HH jets posed a difficult conundrum: how to account for their characteristic low-excitation spectra, which indicate shock velocities of at most a few tens of kilometers per second, in the face of their supersonic bulk velocities of several hundred kilometers per second. The earliest suggestion that jets might consist of a series of highly oblique (hence weak), stationary, recollimation shocks of the kind seen in laboratory jets (e.g., Falle et al. 1987, Cantó et al. 1989) had to be abandoned when it was recognized that the knots in many jets exhibit large proper motions (see Section 3.1). This has left two competing theories for the origin of the knotty structure and low-excitation nature of jets. On the one hand, a series of oblique, traveling shocks may be excited in the jet by hydrodynamic (e.g., Bührke et al. 1988, Stone et al. 1995, 1997, Hardee & Stone 1997, Micono et al. 1998b,c), magnetohydrodynamic (e.g., Ouyed & Pudritz 1997, Goodson et al. 1997, Frank et al. 1998, Cerqueira & de Gouveia Dal Pino 1999, Stone & Hardee 2000), or thermal (de Gouveia Dal Pino & Opher 1990) instabilities. On the other hand, variations in the velocity of the flow may generate internal working surfaces that propagate along the jet and have shock velocities comparable to the amplitude of the velocity perturbation (e.g., Raga et al. 1990, Kofman & Raga 1992, Raga & Kofman 1992, Hartigan & Raymond 1993, Stone & Norman 1993, Falle & Raga 1993, de Gouveia Dal Pino & Benz 1994, Falle & Raga 1995, Raga & Noriega-Crespo 1998). These two models predict very different internal structures for the knots [e.g., compare Micono et al. (1998b,c) and

Raga & Noriega-Crespo (1998)]. However, given the typical knot sizes of 1 arcsec or smaller, *HST* images are required to differentiate between the two alternatives.

To date, six collimated jets have been observed with HST: the HH 1 jet (Hester et al. 1998, Reipurth et al. 2000a), the HH 30 jet (Burrows et al. 1996, Ray et al. 1996), the HH 34 jet (Ray et al. 1996), the HH 47 jet (Heathcote et al. 1996), the HH 111 jet (Reipurth et al. 1997b, 1999), and the L1551 IRS 5 jet (Fridlund & Liseau 1998). The HH 1, HH 34, and HH 111 jets are prototypical examples of rather straight, knotty jets and are in general similar to one another. The HH 34 jet can be traced essentially all the way back to its source, whereas most other jets suffer significant extinction near their sources. Figure 5 shows a mosaic of optical and infrared (IR) HST images of the visible HH 111 jet and its highly obscured source region.

3. KINEMATICS OF HH FLOWS

3.1. Proper Motion Measurements

When George Herbig and collaborators in the early 1980s recognized the high proper motions of HH objects, they opened up a field of study with enormous impact on our understanding of HH flows (e.g., Cudworth & Herbig 1979, Herbig & Jones 1981, 1983, Jones & Herbig 1982). Tangential velocities can be derived from well-sampled ground-based images taken at several epochs under excellent seeing conditions, and proper motions have been determined for numerous HH objects (e.g., Heathcote & Reipurth 1992, Eislöffel & Mundt 1992, 1994, Eislöffel et al. 1994b). Typical tangential velocities of jets from low-luminosity sources are of the order of 100–200 km s^{-1} with a very large spread [velocities as high as 500 km s^{-1} have been measured in the HH 111 jet (Reipurth et al. 1992)]. If the source locations are known, these measurements directly determine the dynamical ages of the individual HH objects independent of the flow-inclination angle.

Ground-based proper motion studies are limited in two ways. First, such data can only provide bulk motions, given the poor spatial resolution achieved from the ground. Second, poor resolution requires relatively long time intervals between images; for the nearest HH objects ($\approx$140 pc), time intervals around 4–5 years are required, extending to several decades for more distant objects. This is comparable to the postshock cooling times in the flows, and HH objects can exhibit significant variability on such timescales, with some structures fading and new knots emerging (e.g., Herbig 1969, 1973). The only way to avoid confusing physical motion with photometric variability is to decrease the time interval between images, and this requires much improved resolution. By providing an order of magnitude better resolution, observations with HST have ushered in a new era of precision proper motion determinations using images obtained only a few years apart, shorter than typical postshock cooling times, e.g., HH 152 (Krist et al. 1999). The uncertainties in these HST-based measurements are now comparable to what is induced by uncertainties in the distances to the objects.

Several trends are apparent in these data. (*a*) The jets in these HH complexes often exhibit large flow velocities and small velocity dispersions. (*b*) The tangential velocities tend to decline with increasing distance from the flow axes. (*c*) In the large bow shocks lying downstream from the jets, the bow tips tend to have the fastest motions while the bow skirts move more slowly. (*d*) In some complex flows, such as HH 2, both downstream- and upstream-facing bow shocks are found. The downstream-oriented shocks tend to have large proper motions, whereas the reverse-facing shocks are always slow moving or stationary.

Besides the physical information provided by proper motion measurements, such data also have several practical uses. First, the orientations of proper motion vectors provide the most precise means of linking candidate protostellar sources to specific HH objects (e.g., Devine et al. 1999c). Second, HH flows seen within the chaotic structures of HII regions, from which they are often indistinguishable, can be securely identified by comparing multi-epoch images (e.g., Bally et al. 2000).

3.2. Radial Velocity Measurements

Long-slit spectroscopy is ideally suited to measuring radial velocities along the axes of collimated jets and, additionally, provide line widths, excitation conditions, and electron densities (see Section 9). Numerous HH jets have been studied in this manner (e.g., see Meaburn & Dyson 1987, Mundt et al. 1987, Bührke et al. 1988, Reipurth 1989a,b, Mundt et al. 1990a, Hartigan et al. 1990, Heathcote & Reipurth 1992, Morse et al. 1993a, Fridlund & Liseau 1994, López et al. 1996, Reipurth et al. 1997b). The bulk radial velocities are generally high, of the order of 100–200 km s^{-1}. While internal velocity dispersions are often seen, they are typically small compared with the bulk flow velocity. The low-excitation [SII] knots in the jet bodies are associated with small-amplitude-velocity jumps; for example, in the HH 34 jet, the widths of the [SII] 6717/6731 lines are less than 30 km s^{-1} (Bührke et al. 1988). Large Hα-bright bow shocks tend to be associated with larger-radial-velocity discontinuities. When ordered motion is found, it tends to have a gentle decrease in velocity as the jet flows away from the source, although one case of a major increase in velocity is known (Reipurth 1989b).

When studying the HH 24 jet, Solf (1987) noted a splitting of the lines near the source, with a high-velocity component having a gentle velocity decrease along the flow axis, and a weaker, lower-velocity component with a steep acceleration. He interpreted this in terms of an inner fast jet flow surrounded by a coaxial envelope of entrained material. Because of their interaction, the fast jet slows down slightly as the ambient material is being accelerated. Such double kinematical signatures have now been found in several other jets [e.g., HH 34 (Bührke et al. 1988), HH 47 (Hartigan et al. 1993), and HH 111 (Reipurth et al. 1997b)]. The resulting mixing layers have been studied theoretically by various authors (e.g., Stahler 1994, Raga et al. 1993, Binette et al. 1999). Figure 6 shows a long-slit echelle spectrum along the HH 111 jet.

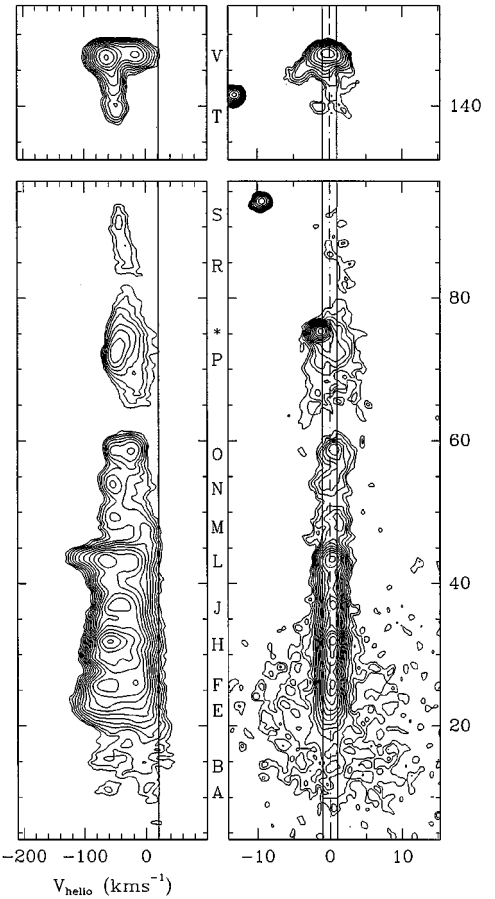

Figure 6 Long-slit spectrum of the [SII] 6717/6731 lines along the body of the HH 111 jet shows large velocity dispersions at bow shocks. Two velocity components are seen at the base of the jet, where ambient material is accelerated and jet material is decelerated. (*Vertical line*) The rest velocity of the ambient medium is indicated by a vertical line. The scale on right is in arc seconds. [From Reipurth et al. (1997b)]

3.3. Kinematics of Bow Shocks and Jets

Though long-slit techniques work well for the analyses of linear features such as jets, they are inefficient in the study of bow shocks and other extended structures. Fabry-Perot spectrometers and image slicers (integral field spectrographs) are coming into increasing use in the characterization of the radial-velocity fields of HH objects (Morse et al. 1992, Lavalley et al. 1997, O'Dell et al. 1997a, Rosado et al. 1999b, Hartigan et al. 2000c). Such observations clearly show large line widths and high velocities toward the apices of bow shocks, with decreasing flow speeds

toward the bow shock wings. Furthermore, the division of a working surface into a two-shock structure with a bow shock and a Mach disk, which was initially noted on morphological and excitation grounds (Section 2), has been confirmed kinematically in several large working surfaces (Morse et al. 1992, 1993b, 1994). The physical parameters derived from Fabry-Perot maps allow a determination of the jet-to-environment density ratio by balancing the ram pressures at the Mach disk and bow shock. Such measurements show that HH jets are about an order of magnitude denser than the surrounding medium.

When tangential and radial velocities of a jet are combined, the flow inclination to the plane of the sky can be derived. As an example, Heathcote & Reipurth (1992) derived an angle of 31° to the plane of the sky for the Mach disk in HH 34, and an angle of 28° for the HH 34 jet, and Morse et al. (1992) found the same angle for the HH 34 jet.

4. SPECTROPHOTOMETRIC STUDIES

4.1. Optical Line Ratios and Shock Models

The early spectroscopic studies of HH objects established their peculiar nature, setting them apart from usual photoionized nebulae (e.g., Böhm 1956). Since then, major compilations of line fluxes from a variety of HH objects have been obtained (e.g., Brugel et al. 1981a, Solf et al. 1988, Böhm & Solf 1990, Hartigan et al. 1999). In the following, we discuss the current status of spectrophotometric studies of HH objects [for reviews of the early development of the subject, see Schwartz (1983a) and Böhm (1990)].

HH objects are broadly divided into high- and low-excitation objects [see Böhm (1983) for a detailed definition]. Two easily measured excitation parameters are the flux ratios [OIII] 5007/Hβ and [SII] (6717 + 6731)/Hα, which permit the definition of quantitative limits between well-defined categories of high-, intermediate-, and low-excitation HH objects (Raga et al. 1996). Prototype high- and low-excitation objects are HH 1 and HH 7, respectively. Both of these line ratios are insensitive to reddening because of the proximity of the lines. However, interpretations of line ratios in HH objects generally depend on a proper correction for reddening because of the high extinction often suffered by these objects. Miller (1968) noted that the ratio of the [SII] 4068/4076 to the [SII] 10318/10337 lines provides a measure of the reddening. These lines originate from the same upper level so their theoretical ratio is fully determined by the ratios of their transition probabilities and frequencies [for details on this and other methods, see Solf et al. (1988)].

Although HH flows are predominantly emission line objects, they do have very weak blue continua, which rise into the ultraviolet (UV) (e.g., Böhm et al. 1974, Brugel et al. 1981b, Solf et al. 1988, Hartigan et al. 1999). These blue continua are usually attributed to collisionally enhanced two-photon decay in neutral atomic hydrogen (Dopita et al. 1982a, Brugel et al. 1982). But a continuum peak around

λ1580 may also be due to H_2 fluorescence (Böhm et al. 1991). Although such continua are weak, their integrated intensity is large enough to make them an important coolant in low-velocity shocks, with fluxes up to 50% of Lyα (Hartigan et al. 1999).

The recognition that shocks play a fundamental role in the emission from HH objects (Schwartz 1975, 1978) enabled a physical interpretation of the intensities, ratios, and profiles of their emission lines. Observed line ratios were initially compared with plane-parallel models (Dopita 1978, Raymond 1979), indicating shocks with velocities up to 70–100 km s^{-1} moving into a low-density, almost neutral, medium. However, such models cannot simultaneously accommodate the presence of low-excitation lines such as [OI] and [SII] and highly ionized species such as [OIII] and [CIV]. Bow-shock models, on the other hand, naturally produce a range of shock velocities, with high-excitation lines produced at the apex and increasingly lower-excitation lines formed where the shocks become more oblique along the bow wings. Here, only the velocity component perpendicular to the bow becomes thermalized (e.g., Hartmann & Raymond 1984, Hartigan et al. 1987, Raga et al. 1988, Raymond et al. 1988, Noriega-Crespo et al. 1990).

Simple analytic formulae provide the shock velocity and flow orientation from a single well-resolved profile of a low-excitation line (Hartigan et al. 1987). Furthermore, position-velocity diagrams extracted from long-slit spectra provide a powerful diagnostic tool for interpreting the kinematics, orientation, and physical conditions in the recombination regions of HH flows. Excellent fits between spectra and models have been achieved for many flows (e.g., Choe et al. 1985, Raga & Böhm 1985, 1986, Raga et al. 1986, Solf et al. 1986, Hartigan et al. 1990).

Despite these evident successes in interpreting the general spectra of HH objects, a number of disconcerting discrepancies between observations and shock models persist (Böhm 1995). Raga et al. (1996) compiled all available spectra for 45 separate condensations in 31 different HH flows and found that 53% are high-excitation objects, 29% are intermediate-excitation objects, and 18% are low-excitation objects. Line ratios in low-excitation objects are well reproduced by single planar shock models with a narrow range of shock velocities around 30 km s^{-1}. For intermediate-excitation objects, inconsistencies emerge, with various line ratios within a single object suggesting shock velocities between 30 and 100 km s^{-1}. For all high-excitation objects, the line ratios of [OIII] 5007 and [NeIII] 3868 to Hβ indicate shock velocities that never exceed 100 km s^{-1}, which suggests that a mechanism might exist that limits the maximum shock velocity in high-excitation objects. These unexpected results suggest that our understanding of HH shocks may be less secure than has been believed.

Line ratios are influenced not only by the shock structures but also by abundance variations. It is generally assumed that the gas-phase abundances of refractory elements like Fe or Ca are considerably depleted in molecular clouds because of their condensation into dust grains. When overtaken by a sufficiently strong shock, it is expected that these grains are destroyed, thus returning the Fe and Ca to the gas phase (McKee et al. 1987, however, see Mouri & Taniguchi 2000). Therefore,

high-excitation HH objects should have high gas-phase Fe and Ca abundances typical of Population I compositions, whereas in low-excitation objects, these elements might still partially remain in dust grains. In a series of studies, Beck-Winchatz et al. (1994, 1996) and Böhm & Matt (2001) have determined metal abundances for 21 HH flows and find that, although the high-excitation objects indeed show little or no depletion, unexpectedly neither do the low-excitation objects. This suggests that at some point in their evolution, the material in all HH objects has passed through strong shocks, possibly related to processes in the jet-launch region.

4.2. Ultraviolet Observations

After the discovery of strong UV emission lines and continua in HH objects (Ortolani & D'Odorico 1980, Böhm et al. 1981), most of the UV work on HH objects was done in the 1980s, when the IUE satellite was still active (see Böhm et al. 1993 and references therein). Since then, only a few studies have appeared, but major advances are soon expected with the Space Telescope Imaging Spectrograph.

Strong UV lines provide significant cooling in HH objects. As an example, Figure 7 shows a UV-optical spectrum of HH 47A from Hartigan et al. (1999). In high-excitation objects, more energy may be emitted in the UV than in the optical, principally through the lines of [CIV] 1548/1551 and [CIII] 1907/1909 (e.g., Böhm et al. 1987); in low-excitation objects, on the other hand, fluorescent lines in the Lyman bands of the H_2 molecule can be prominent (e.g., Schwartz 1983b, Curiel et al. 1995, Raymond et al. 1997). Additionally, the blue continuum seen in HH objects increases toward the UV, with a peak around 1575 Å, and is also believed to be due to collisionally enhanced two-photon decay in neutral atomic hydrogen (Brugel et al. 1982), although fluorescent H_2 may also play a role at the shortest wavelengths (Böhm et al. 1987).

Accurate spectrophotometry in the UV is hampered by the large extinction that many HH objects suffer. But although the amount of extinction can be determined using the Miller (1968) method, the shape of the extinction curve may differ from region to region (e.g., Böhm-Vitense et al. 1982). Even disregarding such problems, some UV lines pose puzzles. For example, the [CIV] line never shows a shock velocity exceeding roughly 100 km s^{-1}, and the [NV] 1240 Å line, which should be very strong, has never been seen in an HH object. Additional complications for modeling comes from the considerable variability in UV line and continuum emission that has been documented in several objects on short timescales (e.g., Brugel et al. 1985, Liseau et al. 1996a).

5. INFRARED OBSERVATIONS OF HH FLOWS

With the major advances in IR detector technology during the past decade, a new window has opened up for research into HH flows. The main cooling in HH shocks at near-IR wavelengths is due to emission from molecular hydrogen. The study of

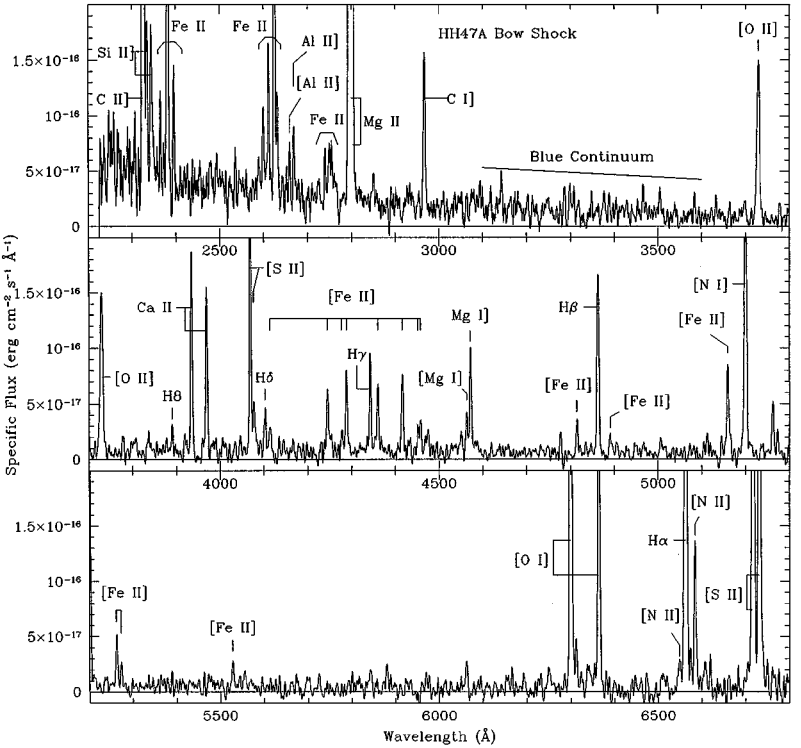

Figure 7 An optical/ultraviolet spectrum of the HH 47A Mach disk taken with the faint-object spectrograph aboard the Hubble Space Telescope. The strongest line in the spectrum is the MgII 2800 doublet, which is several times brighter than Hα. [From Hartigan et al. (1999).]

molecular emission lines offers insights into the physical regimes of low-velocity shocks that are complementary to those probed by atomic and ionic lines. In addition to numerous H_2 lines, HH objects also emit several strong emission lines of [FeII] in the near-IR wavelength region.

Narrow-band filter imaging is a powerful tool for identifying shock-excited near-IR emission nebulae in the vicinity of very young embedded stars (e.g., Hodapp 1994, Aspin et al. 1994, Yu et al. 1997, Garnavich et al. 1997, Stanke et al. 1998). Some of these nebulae coincide with known HH objects, but most do not. Particularly interesting regions with numerous such H_2 and [FeII] nebulae are found around several Class 0 sources in the L1448 cloud (Eislöffel 2000, Wolf-Chase et al. 2000), in the Serpens cloud (Hodapp 1999), and in the OMC 2/3 clouds (Yu et al. 2000). The most straightforward explanation is to simply assume that such IR line-emitting nebulae are parts of HH flows suffering significant amounts of extinction. Although this interpretation in certain specific cases is

highly probable, it has not been rigorously established as a general rule. Both optical and IR spectroscopy of HH flows have revealed a wide range of excitation conditions and a bewildering range of line ratios. It is currently not possible to predict the IR spectrum of an HH object based on its optical spectrum. Significantly more work is required before we fully understand the nature of IR emission processes in outflow regions.

A wealth of IR studies of outflows from young stars exists by now, and Reipurth (2001) lists more than one hundred such references. The reader is referred to this list for a complete bibliography.

5.1. Near-Infrared Spectroscopy

The early work on molecular hydrogen in HH objects, based on very-low-resolution spectra, revealed that most HH objects are detected in H_2, with a tendency for low-excitation HH objects to be brighter in these IR lines (e.g., Elias 1980, Schwartz et al. 1987, Wilking et al. 1990). The near-IR spectra of HH objects are dominated by molecular hydrogen lines that arise from low-lying vibrational levels in the H_2 electronic ground state. The brightest, easily observable line is the 1-0 S(1) line at 2.122 μm, which often has a flux comparable to the Hα line in the same object. The Q-band lines are even brighter, but they are hard to observe from the ground because of terrestrial H_2O. Near-IR spectra covering a range of H_2 lines allow insights into the excitation mechanism because the lines are optically thin, and line intensities provide column densities in a number of excited states. It is widely accepted that IR H_2 lines in HH objects are collisionally excited in shocked gas at a temperature of a few thousand degrees kelvin, as already discussed in the pioneering paper by Elias (1980). Such thermal excitation will populate only the lowest vibrational levels ($v \leq 3$). Many other excitation mechanisms have been discussed, in particular fluorescence pumped by UV photons (e.g., Fernandes & Brand 1995). In a UV spectrum of HH 43, Schwartz (1983b) observed a number of fluorescently excited H_2 lines, but so far no IR HH spectra with good resolution have conclusively shown H_2 lines from the high ($v \geq 3$) populational levels fluorescence should produce (Gredel 1994, Schwartz et al. 1995). Medium-resolution spectra have been obtained toward a number of HH objects, and in all cases, the inferred population distribution is thermal and can be described by an excitation temperature in the range 2000–3000 K (e.g., Gredel et al. 1992, Gredel & Reipurth 1993, Gredel 1994, 1996, Everett 1997, Fernandes 2000, Eislöffel et al. 2000b). Other mechanisms could contribute to this excitation, and Wolfire & Königl (1991) have presented comprehensive calculations of various processes and useful diagnostics to discriminate between them.

Both J-type (jump) and C-type (continuous) molecular shocks (Draine1980) have been invoked to explain the IR line spectra of HH objects (e.g., Hollenbach 1997). In both cases, the molecules are heated and accelerated, but the shocks are mostly nondissociative. C-shocks require a magnetized medium at low ionization (e.g., Smith 1993), whereas J-shocks require a medium in which magnetic fields

are weak or absent, or where shock speeds are significantly higher than the Alfvén speed (e.g., Hollenbach & McKee 1989, Smith 1994a). In C-shocks, the low level of ionization largely decouples the neutrals from the magnetic field, so the heating and acceleration occurs by collisions between neutral particles and the charged particles tied to magnetic field lines. This ambipolar heating occurs throughout a thick layer as the neutrals are gradually heated by the ions, thus washing out the sharp discontinuity found in J-shocks. The temperatures in C-shocks typically reach at most a few thousand degrees, so many molecules are preserved. In this environment, a rich molecular chemistry may unfold, as observed in selected outflow regions (e.g., Bachiller & Tafalla 1999). In contrast, for J-shocks, the shock front is about one mean free path wide, and the higher-velocity shocks ($v_s \geq 40$–50 km s^{-1}) dissociate ambient molecules. Also, the UV radiation produced by J-shocks with $v_s \geq 60$ km s^{-1} can form a UV precursor that may predissociate or preionize the preshock gas.

It is often not easy to identify which type of shock dominates in a given HH object. This is partly because the shocks in HH flows mostly have complicated shapes, which permit a range of effective shock velocities to coexist. Long-slit spectra across HH flows have revealed excitation changes related to the shock geometry (Eislöffel et al. 2000b), as also seen in IR images (see below). To discriminate between the various excitation mechanisms, numerous near-IR emission lines with very large spreads in excitation temperatures are needed (e.g., Gredel 1994, 1996, Eislöffel et al. 2000b). Overall, observations of HH flows suggest that most shocks are C-type, but with some cases of J-shocks, and that sometimes the two types coexist (e.g., Smith 1994b, Hartigan et al. 1996, Everett 1997).

The rich IR emission line spectrum of [FeII] offers an excellent opportunity to study the ionized component of the shocked gas in HH objects. Virtually all the [FeII] lines in the 1.1- to 2.5-μm region arise from the a^4D term, which has four levels that are closely spaced, so transitions from them are relatively insensitive to temperature. A variety of density-sensitive line ratios exist and are discussed by Oliva et al. (1990) and Bautista & Pradhan (1996, 1998). Because the [FeII] lines have a much larger critical density than [SII] and [OII], they provide an interesting complement to these two more commonly employed density tracers. For temperature determinations, transitions from levels with very different energies above ground are required, and therefore, near-IR studies must be supplemented by optical or mid-IR spectra. An interesting temperature diagnostic is the ratio of the 8617 Å line to the 1.644 μm line; the former was found to be bright in the HH 34 jet (Reipurth et al. 1986) but is otherwise little studied in HH objects. There are several bright [FeII] lines in the J and H windows that arise in the same upper level, in particular the lines at 1.257 μm and 1.644 μm, and their ratio is therefore sensitive to reddening (e.g., Gredel 1994).

As in the optical part of the spectrum (Section 4.1), high-spectral-resolution studies of IR lines provide important insights into the kinematics and geometry of the shocks (e.g., Schwartz & Greene 1999). However, only a few studies of IR lines from HH flows have been made with sufficient resolution to determine

line profiles (e.g., Zinnecker et al. 1989, Carr 1993, Tedds et al. 1999, Yu et al. 2000, Davis et al. 2000a,b). The recent availability of IR Fabry-Perot imagers and echelle spectrographs should greatly expand such data sets for comparison with theoretical line profiles and provide data of the same quality as already exist in the optical.

5.2. H_2 and [FeII] Images

It is interesting to compare optical images of HH flows with IR images of their H_2 emission (e.g., Schwartz et al. 1988, Hartigan et al. 1989, Gredel & Reipurth 1994, Davis et al. 1994a,b, 1995, Hartigan et al. 2000b). Further insight into the nature of shocks is provided by the spatial distribution of H_2 versus [FeII] emission, and many studies present comparisons between narrow-band filter images transmitting the H_2 2.122 μm and [FeII] 1.644 μm lines (e.g., Lane 1989, Stapelfeldt et al. 1991, Gredel 1994, Eislöffel et al. 1994a, Schwartz et al. 1997, Davis et al. 2000b). Such comparative studies reveal complex spatial relationships between the molecular and ionized species. For bow shocks, there is a tendency for regions of higher excitation as traced by [FeII] to be located nearer the apex, where the velocity component normal to the shock front is a maximum. On the other hand, H_2 emission is preferentially found along the bow wings, where the normal component of the velocity decreases. Presumably H_2 is dissociated except where the shock is sufficiently oblique and, thus, weaker.

Low-excitation HH objects frequently have strong H_2 emission lines. Examples are HH 91, HH 43, and HH 205-210, which for HH objects are among the brightest known H_2 emitters (Gredel et al. 1992, Schwartz et al. 1988, Allen & Burton 1993). But these flows are unusual. For example, the HH 34 jet, which has extremely low excitation, hardly emits any H_2 (e.g., Stapelfeldt et al. 1991, Stanke et al. 1998). However, a similarly well-collimated jet, HH 212, is extremely bright in H_2 (Zinnecker et al. 1998). The density of these two jets may differ and may be high enough in HH 212 to allow the formation of molecules faster than they are dissociated. An additional difference could also be the degree to which the jets are embedded, with the HH 34 jet moving into a tenuous, mostly atomic medium while the HH 212 jet is passing through a relatively dense molecular environment. The abundance of H_2 molecules not only within but also surrounding an HH jet might be critically important for the resulting spectrum. Where HH jets move through molecular material, H_2 may be the principal IR coolant, but otherwise the basic near-IR emitter of an HH jet may be [FeII] (Reipurth et al. 2000b).

Proper motion studies based on IR H_2 emission are now beginning to appear, and in many cases, high velocities of hundreds of kilometers per second are observed (e.g., Noriega-Crespo et al. 1997, Micono et al. 1998a, Coppin et al. 1998, Chrysostomou et al. 2000). The existence of H_2 molecules at such high velocities would seem to suggest that the shocks are formed as internal working surfaces, where faster-moving material catches up with previously ejected slower-moving gas.

5.3. Mid- and Far-Infrared Spectroscopy

Very little work has been done so far on the mid-IR emission from HH objects. Using ISO SWS spectra, Neufeld et al. (1998) detected HH 54 in the S(1)-S(5) pure rotational lines of H_2 between 6.91 and 17.0 μm and demonstrated that departures from equilibrium of the ortho- to para-H_2 ratio can serve as a chronometer for the period during which the gas has been warm. Using ISOCAM, Noriega-Crespo et al. (1998) mapped the HH 337 region in the Cep E outflow in the 6.91- and 9.66-μm lines of molecular hydrogen.

It has been known for some time that the fine-structure [OI] emission line at 63 μm is bright in HH objects, based on spatial coincidence and radial velocity (Cohen et al. 1988). ISO LWS spectra of HH objects covering the wavelength region from about 45 to 190 μm have been recently obtained. In many objects, [OI] 63 μm is the only emission spatially coincident with the HH flows, implying that far-IR cooling of HH objects is strongly dominated by this line (Liseau et al. 1997, Nisini et al. 1999, Benedettini et al. 2000). Three interesting exceptions are the HH 54 object—which displays a rich spectrum with high-J rotational CO lines, with thermal water emission, and with OH lines (Liseau et al. 1996b, Nisini et al. 1996)—and the HH 7 objects and HH 80/81 (Molinari et al. 2000, 2001). When outflow material goes through a dissociative J-shock, the [OI] 63-μm emission is an excellent measure of the mass-loss rate from the driving source (Hollenbach 1985, Ceccarelli et al. 1997). Finally, Molinari et al. (1999) detected significant far-IR continuum between 10 and 200 μm in HH 7, which suggests that thermal emission from dust grains may be important in some HH objects. They additionally detected a broad feature between 50 and 70 μm ascribed to crystalline H_2O ice originating from dust processed by the HH 7 shock. Evidence for dust in HH objects has been scarce (e.g., Henney et al. 1994), and it has generally been believed that the shocks within HH flows destroy almost all grains. However, recently Mouri & Taniguchi (2000) have argued that significant amounts of dust may survive in shocks.

With the advent of SOFIA and SIRTF, the mid- and far-IR wavelength range will undoubtedly become a more important source of information on HH flows than it has been so far.

6. THE REGION OF JET LAUNCH

6.1. Theoretical Considerations

A detailed discussion of the launch and collimation of outflows is beyond the scope of this review (for recent reviews, see Shu et al. 2000, Königl & Pudritz 2000, Eislöffel et al. 2000a). Here, we summarize the main issues that affect our understanding of HH flows. It is clear that outflows are ultimately powered by the release of gravitational potential energy liberated by matter accreting onto a forming star. Comparing the mechanical and bolometric luminosities of outflow sources indicates that mass loss carries away about 10% or less of the energy

released by accretion (Cabrit et al. 1990, Cabrit & André 1991, Hartigan et al. 1995). The rest is released as radiation. Furthermore, it is likely that the acceleration of an outflow and its collimation occur at different locations and perhaps even by different processes. While most flows are probably launched at radii of at most a few astronomical units, most HH jets appear to have beams that are 50–500 AU wide at the point where they first become visible, indicating that collimation occurs at larger distances from the source than the launch region.

Thermal and radiation pressures appear to play important roles in the launch of flows only in high-luminosity sources since in low-luminosity protostars the outflow momenta are typically one to two orders of magnitude larger than the momentum in the radiation field (Lada 1985). Thus, for most low-luminosity, young stellar objects (YSOs), magnetohydrodynamic or magnetocentrifugal processes are usually invoked to launch the outflow (Blandford & Payne 1982, Pudritz & Norman 1983, Uchida & Shibata 1985, Shu et al. 1988, Camenzind 1990, Königl & Ruden 1993, Contopoulos & Lovelace 1994, Shu et al. 1994a,b, Goodson & Winglee 1999). Purely hydrodynamic acceleration and collimation models (Frank & Mellema 1996) are not widely favored.

Outflows can in principle originate in three generic locations near the source: (*a*) as a "normal" stellar wind launched from the star itself; (*b*) as an "X-wind" launched from the stellar magnetosphere at a few to tens of stellar radii, where it interacts with the inner edge of the accretion disk; and (*c*) as a magnetocentrifugal "disk wind" launched from the accretion disk at distances of 0.1 AU or more from the young star. Flow acceleration can be further subdivided into dynamic and static models. Dynamic models produce short-duration (comparable to the orbital time at the launch point) but powerful outbursts (Uchida & Shibata 1985, Lovelace et al. 1997, Goodson et al. 1999), whereas static models power steady-state winds (Pudritz & Norman 1983, 1986, Lovelace et al. 1993, Shu et al. 1994a,b).

Most launch mechanisms produce wide-angle flows. In principle, the cavity produced by the wind in the surrounding medium can act as a nozzle to collimate this wind into a jet. Such purely hydrodynamic nozzles can form if the density gradients in the medium are clearly stratified (Königl 1982, Raga & Cantó 1989, Frank & Mellema 1996, Mellema & Frank 1997). But a wind can only be collimated by the medium if the flow ram pressure normal to the cavity surface is comparable to or less than the pressure in the confining medium. Since the flow ram pressure tends to be very large near the launch region, but declines as the inverse square of the distance from the YSO, hydrodynamical collimation becomes plausible only at relatively large radii ($\gg$10 AU) for typical flow and envelope parameters. However, infall motions in the envelope at speeds comparable to the local gravitational escape velocity may substantially increase its ability to deflect and collimate a wind into a jet (Delamarter et al. 2000). Furthermore, hydrodynamical collimation may be transient. For example, the shocks driven into a stratified medium by the advancing wind can deflect the outflow as it propagates through the envelope. However, such dynamical collimation would cease once the envelope is swept out of the way.

Magnetic fields have been invoked to increase the pressure and rigidity of the surrounding medium. In some models, flow collimation is a direct result of the magnetic geometry and does not require an external medium. In the models of Lovelace et al. (1993) and Shu et al. (1995), the magnetic field tends to align with the rotation axis of the disk and star at large radii and collimates the wide-angle flow into a jet. In the Shu et al. models, the "jet" is the high-density core of the flow moving along the rotation axis of the system. The hour-glass–shaped, pinched-field geometry produced by rotation and collapse also tends to collimate the flow at large radii in the disk wind models. In some models, rotation of the system wraps up the field to generate a toroidal component above and below the disk even if the field is initially parallel to the rotation axis of the system. Such "hoop stress" may be the most efficient means by which to collimate wide-angle flows into jets (Königl 1989, Pelletier & Pudritz 1992, Appl & Camenzind 1993, Heyvaerts & Norman 1989, Ostriker 1997, Mellema & Frank 1997, Lery et al. 1998). Evidence for strong magnetic fields hundreds of AU from a protostar is provided by circular polarization of the radio continuum emission from the vicinity of T-Tau (Ray et al. 1997).

6.2. Radio Continuum Observations

Since extinction is the principal barrier to observing the jet launch region, it follows that interferometric techniques at radio wavelengths should offer an excellent opportunity for such studies.

Only a small number of HH objects have been detected in the centimeter radio-continuum (Pravdo et al. 1985, Rodríguez & Reipurth 1989, Yusef-Zadeh 1990, Anglada et al. 1992). However, various surveys at 3.5 cm have shown that it is common for their energy sources to be detected (e.g., Bieging et al. 1984, Rodríguez & Reipurth 1996, 1998, Anglada et al. 1998). High-angular-resolution observations on scales of tenths of an arcsecond of the brighter HH sources (e.g., HH 1, HH 111) have revealed tiny collimated thermal radio jets extended along the HH jet axes (Figure 8), but unresolved in the transverse direction, implying jet widths of fewer than 50 AU (e.g. Rodríguez et al. 1990, 2000, Rodríguez & Reipurth 1994). The planned EVLA may provide the needed resolution to fully resolve these jets.

At centimeter wavelengths, the continuum emission observed from ionized collimated YSO outflows is mainly due to free-free radiation. Reynolds (1986) calculated the radio continuum spectrum expected from a confined thermal radio jet with constant temperature, velocity, and ionization fraction. For the simple case of a jet with constant opening angle, the frequency dependence of the flux density is $S_\nu \propto \nu^{0.6}$. A few collimated radio jets from embedded young stars have nonthermal spectra ($S_\nu \propto \nu^\alpha, \alpha \leq 0$), (e.g., Curiel et al. 1993). Such nonthermal jets are not easy to understand but may involve diffusive shock acceleration processes (Crusius-Wätzel 1990, Henriksen et al. 1991). For further details on radio jets, see the reviews by Anglada (1995) and Rodríguez (1997).

6.3. Collimation of Jets

Observational insights into the mechanism(s) of jet collimation are hard to come by. Despite their extremely high resolution, the radio continuum observations discussed in the previous section do not resolve the widths of the jets. Therefore, indirect information must be sought about the jet launch region and can in principle be gathered by studying the rate of expansion of jets close to their sources. Opening angles of HH jets from ground-based images have been obtained by Raga et al. (1991) and Mundt et al. (1990b). These observations suggest that, rather than having a constant opening angle, jets expand rapidly in the unobservable region very close to their sources, followed by the much slower expansion commonly seen at larger distances. More accurate expansion rates of HH jets have been measured with HST (e.g., Ray et al. 1996, Hester et al. 1998, Reipurth et al. 2000a,b), which suggests a rapid jet expansion close to the source (Figure 9). Spectroscopic analysis of microjets (see below) cast further light on the opening angles of outflows from T Tauri stars [for further details, see Mundt et al. (1990a), Eislöffel et al. (2000a)].

It is not clear precisely how these results can be related to theoretical models of jet launch and collimation. The observed jet widths may represent the extent

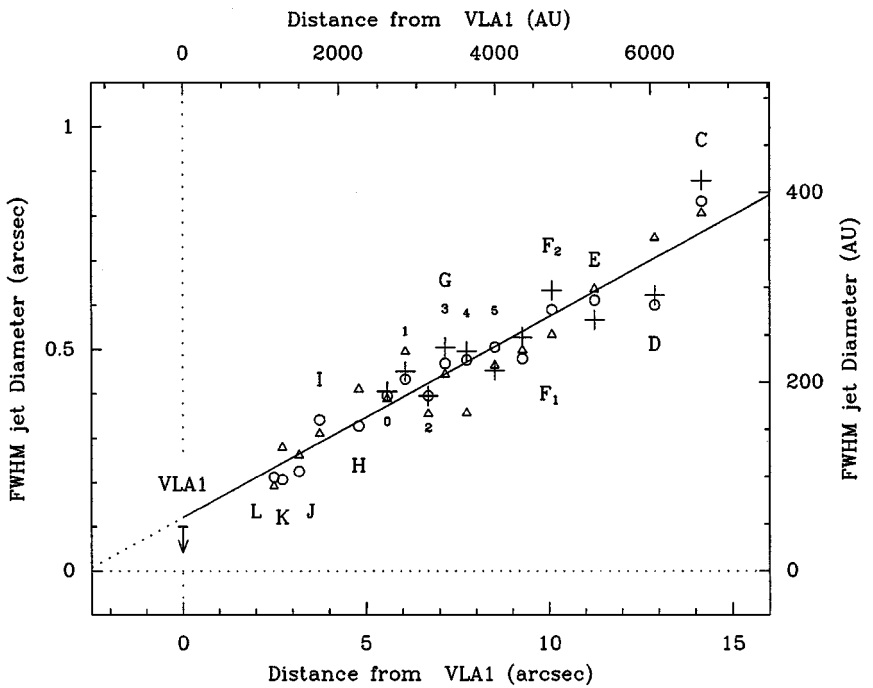

Figure 9 The deconvolved FWHM jet diameter along the HH 1 jet as a function of distance from the driving source. Based on images of [FeII] (*circles*), H_2 (*triangles*), and [SII] (*pluses*) from the Hubble Space Telescope. [From Reipurth et al. (2000a).]

of wings of bow shocks, where material from internal working surfaces splash sideways, so that the "true" jets could be much narrower. Such issues need to be understood before the observed expansion rates can be properly interpreted.

6.4. Masers Around Jet Sources

Observations over the past decade have shown that weak water-maser emission at 22 GHz is relatively common around deeply embedded low-luminosity sources (e.g., Claussen et al. 1996). Water masers can only appear in an environment in which temperatures and densities exceed 200–300 K and 10^8–10^9 cm^{-3}, respectively, as required to sufficiently populate the energy levels responsible for the maser transitions. Because masers can arise near newborn stars in shocked gas, they may provide additional insight into the outflows from such sources. VLBA and VLBI observations offer milliarcsecond resolution, so the positions and radial velocity of the masers can be determined with exceptional precision. In addition, multi-epoch observations allow accurate proper motion determinations of the masers in the outflowing gas. Such data permit accurate determinations of the flow vectors and their inclination to the plane of the sky. The main limitation is that masers are highly nonlinear phenomena that appear and disappear at unpredictable rates. Therefore, data must be continuously obtained so a picture of the outflow can be built up. The best data on an HH jet are those of HH 212 by Claussen et al. (1998), which show a number of masers along the well-defined jet axis. Some masers appear within 40 AU of the source, indicating that jet formation and acceleration takes place within this radius. In the coming years, maser observations may provide important insights into conditions in the jet launch region.

The study of masers around high-mass young stars is better developed, partly because the masers are more frequent and brighter around such sources (e.g., Torrelles et al. 1998, Wilner et al. 1999). Such observations may permit a comparison between the launch and collimations of flows from low- and high-mass stars.

6.5. Micro Jets

Some T Tauri stars display high-velocity forbidden emission lines reminiscent of those in HH objects. Such lines are most often blueshifted, indicative of a flow whose receding part is obscured by a circumstellar disk (Appenzeller et al. 1984, Hartmann & Raymond 1989, Hamann 1994, Edwards et al. 1994, Hartigan et al. 1995). Long-slit spectroscopy of such T Tauri stars sometimes reveals small HH flows with extents of just a few arcseconds, and they are therefore dubbed microjets (Solf 1997). Under the assumption that the very young, deeply embedded stars associated with large-scale HH flows form their jets in much the same way as visible T Tauri stars, microjets may reveal essential information about how jets are launched, despite their diminutive sizes. Direct imaging of microjets is hampered by the presence of the bright star, but with long-slit spectroscopy, it is possible to effectively remove the underlying stellar continuum (Solf 1989). The resulting position-velocity diagrams permit the identification of the kinematical and spatial

features of these jets. In many cases, two components are detected: a low-velocity component (LVC) and a high-velocity component (HVC). These features often have different strengths in various forbidden lines, which strongly suggest that they represent physically distinct components. Kwan & Tademaru (1988, 1995) suggested that the HVC is caused by a high-velocity flow that becomes collimated into a jet that originates from the star or very inner part of the accretion disk, whereas the LVC comes from a slower wind originating from the disk within several AU of the star. The intensities of forbidden lines provide information on the physical conditions that give rise to their excitation. The [OI] λ5577/λ6300 intensity ratio indicates that, in addition to the HVCs and LVCs, a warm disk corona exists with $n_e \sim 10^7$ cm^{-3} and T $\sim$ 8000 K surrounding the inner few astronomical units of the disk (Kwan 1997).

The spatial and kinematic properties of the forbidden emission line regions in a large number of T Tauri stars have been studied with long-slit spectroscopy by Hirth et al. (1994a,b, 1997). They find clear evidence that the HVC is spatially more extended than the LVC. Also, the emission centroid of the HVC is located further from the source (typically 0.6 arcsec) than the LVC. Furthermore, they find that the velocities of the blueshifted and redshifted lobes can differ substantially.

The little HH 158 jet from DG Tau is a particularly well-observed case of a microjet from a visible T Tauri star (Mundt et al. 1987) with both LVC and HVC components (Solf & Böhm 1993). The body of the jet can be traced to about 1.5 arcsec from the source, followed by several tiny bow shocks with high proper motions (Lavalley et al. 1997, Lavalley-Fouquet et al. 2000, Dougados et al. 2000). HST STIS spectra have shown that the density of the jet decreases with distance from the source and also increases toward the flow axis (Bacciotti et al. 2000).

Because of their diminutive sizes and association with visible T Tauri stars, it is often assumed that microjets represent the final stages of collimated outflows as their sources evolve toward the main sequence. Although it is probably true that microjets are vestiges of the general HH phenomenon, it does not necessarily follow that their sources are more evolved. As discussed in the following section, there are mechanisms that can render an otherwise very young star visible.

7. IRRADIATED JETS

An entirely new class of jets from low-mass stars embedded within HII regions and near sources of soft UV radiation has been recently discovered. When photoionized, the physical properties of these irradiated jets may be directly determined using the standard methods developed for the analysis of ionized nebulae, limiting the need to consider the complex nonlinear physics of shocks.

7.1. The Excitation of Irradiated Jets

Reipurth et al. (1998a) identified four Herbig-Haro jets (HH 444, 445, 446, and 447) near the high-mass multiple star system σ Orionis. These flows originate from

visible T Tauri stars apparently suffering very low extinction and not embedded in molecular cloud cores. On the best ground-based images, two of the jet sources (HH 445 and 446) appear to be associated with faint tails of emission line nebulosity that point directly away from σ Orionis. These arcseconds-long (a few thousand astronomical units) cometary structures are reminiscent of the tails associated with the protoplanetary disks (proplyds) embedded in the Orion Nebula (O'Dell et al. 1993, Bally et al. 1998, 2000) and may indirectly indicate the presence of photoablating circumstellar disks (Johnstone et al. 1998). All four jets near σ Orionis are highly asymmetric, with the main beam about 10 times brighter in Hα than the counter jet. In all four cases, the brighter jets face away from the external source of illumination. Cernicharo et al. (1998) and Rosado et al. (1999a) analyze a jet, HH 399, propagating into the photoionized interior of the HII region M20. Unlike the jets near σ Orionis, the source and counter jet of HH 399 are still deeply embedded within molecular gas surrounding the Trifid Nebula.

Bally et al. (2000) found 21 irradiated microjets propagating into the photoionized interior of the Orion Nebula. These flows are launched by young stars embedded within proplyds (externally irradiated circumstellar disks surrounding young stars) (Figure 10). Most of these tiny flows are predominantly one sided, with beam–to–counter-beam intensity ratios of more than 5. Large excitation gradients are observed along the lengths of some of these jets. Near their source stars, where the jet propagates primarily through the mostly neutral gas inside the proplyd ionization front, the jets are brightest in the 6300 Å line of [OI]. However, beyond the proplyd ionization front, the [OI] emission disappears and the jets become brightest in Hα.

Bally & Reipurth (2001) noted five larger irradiated HH flows in the outskirts of the Orion Nebula and additional jets in the immediate vicinity of early B-stars in the NGC 1333 reflection nebula in Perseus. Three of the irradiated HH flows in the Orion Nebula are bipolar but exhibit C-shaped symmetry, with the jet beams and bow shocks bending away from the core of the Orion Nebula by as much as 20°. An outflow from the nebular interior must be deflecting these jets. Masciadri & Raga (2001) have successfully reproduced the bending of these jets when modeling the effect of a side wind on a jet.

A common trait of many irradiated jets is that their central stars are visible, suffer low extinction, and do not appear to be embedded within opaque cloud cores (HH 399 in M20 is an exception). Evidently the external ionizing or soft UV radiation field has photoablated much of the gas that usually surrounds young stars, leaving the star and its circumstellar disk exposed and visible.

The jets emerging from naked young stars in NGC 1333 demonstrate that nonionizing FUV radiation (912 Å $< \lambda <$ 2000 Å) can also efficiently remove much of the obscuring material that normally surrounds young stars before termination of their jet production phase. Most of the NGC 1333 jets are bipolar and several show strong C-shaped bending (Figure 11). However, in contrast to the jets embedded in the Orion Nebula, which bend away from the core of the nebula, the NGC 1333 jets tend to bend toward the cluster core. One possible reason for

this difference may be that, in NGC 1333, the jet sources may be moving through a stationary medium away from the center of the cluster. In contrast, in Orion, the jet sources may be stationary and their jets may be deflected by an outflow from the nebular core. Perhaps the NGC 1333–irradiated jet sources were ejected recently by three-body encounters in the cluster core or by interactions in nonhierarchical multiple-star systems (see Section 12.4).

HH objects have also been found in a number of HII regions and weakly irradiated environments such as the Gum Nebula. The well-known HH 46/47 and HH 120 outflows emerge from small cometary globules that are embedded in the Gum Nebula, whose interior is ionized by ζ Puppis and γ^2 Velorum. Portions of these HH flows are exposed to the Lyman continuum radiation of these massive stars. Although spectra indicate that these flows are predominantly neutral, the outermost bow shock in the HH 46/47 system, HH 47D, shows evidence of being irradiated; this large bow shock is brightest in the $\lambda\lambda$ 3726, 3729 [OII] lines. Analysis of HH 47D indicates that it traces a shock moving into a photoionized medium (Hartigan et al. 1990, Morse et al. 1994). The large HH objects, HH 124 and 125, embedded in the HII region NGC 2264 (Walsh et al. 1992) also show evidence of being irradiated. As with HH 47D, the blue [OII] lines are very bright and, when an extinction correction is applied, dominate the intensities of all other emission lines in the visual portion of the spectrum. Evidently the UV radiation field and shocks favor the production and excitation of [OII] in these HII regions.

The Orion Nebula contains many bright HH objects that appear to be at least partially irradiated by the Lyman continuum radiation of the Trapezium stars. These include the very bright objects HH 201 through 204 (Taylor & Münch 1978, O'Dell et al. 1997a,b). HH 202 through 204 are bright in [OIII] emission and are also detected in the 20-cm radio continuum (Yusef-Zadeh 1990), indicating that they are ionized. A number of additional high-velocity shocks were identified in an HST proper-motion study of the Orion Nebula by Bally et al. (2000). Most of these flows are dominated by [OIII] and Hα emission, with ratios indicating complete ionization. Other HH objects in the Orion Nebula, such as HH 205 through 210 (O'Dell et al. 1997a), appear to be embedded within the mostly neutral photodissociation region behind the Orion Nebula. Consequently, the emission from these HH objects is dominated by low-excitation shock emission in lines such as [OI] and [SII].

7.2. The Physics of Irradiated Jets

The discovery of externally irradiated HH objects creates new opportunities for diagnosing outflow properties. The nonlinear physics of shocks makes the determination of densities in most HH objects difficult. On the other hand, external photoionization permits the electron densities to be easily estimated in irradiated jets. Raga et al. (2000) modeled the propagation of Lyman continuum radiation into an initially neutral jet. Ionization of either the surface or the entire body of the flow produces hydrogen recombination lines such as Hα whose intensity becomes

directly related to the emission measure, and with an estimate of the depth of the emission region, the electron density can be derived. Furthermore, the red [SII] lines can also be used to measure the electron density directly. Measurements of the electron density, velocity field, and flow morphology can then be combined to infer all global flow properties. External radiation fields are likely to illuminate all unshadowed outflow components equally so that the full flow structure can be determined reliably.

The brightness asymmetry observed in most irradiated jets may be a direct consequence of the asymmetry of the protostellar environment. Although in non-irradiated outflows jet/counter-jet asymmetry is usually attributed to extinction, in most externally irradiated systems there appears to be little obscuring material. Thus, the observed asymmetries may result either from differences in the mass loading between the jet beams or from differences in their heating and consequent spreading. The external radiation field may remove more material from a protostellar envelope on the irradiated side than on the shadowed side. Thus, an intrinsically symmetric bipolar jet propagating through this medium may have more material to entrain on the shadowed side of the circumstellar disk. Increased mass loading decelerates the jet beam, reducing its speed below that of the unencumbered counterjet emerging from the irradiated side of the disk.

The surface brightness of emission lines is proportional to the emission measure, $EM = n_e^2 l$, where l is the path length of the line of sight through the emission region. In an ionized jet, the EM depends on the rate at which the jet spreads orthogonal to the flow axis.

There are three plausible models for explaining the brightness asymmetries of irradiated jets. First, for a bipolar jet with unequal speeds but the same mass-loss rates into each beam and a constant jet opening angle, the faster beam will appear fainter by a factor of $(v_f/v_s)^2$ at a given distance from the source (the subscripts refer to the fast and slow beams). Second, if the jet speeds are unequal but each beam spreads laterally at the same speed, then the beams will have different opening angles. This is the case if the sound speed, c_s, in each beam is the same as might be expected if it is regulated by the external radiation field. In this case, the faster beam will have a narrower opening angle, given by $\theta = 2c_s/v_f$, and will appear brighter by a factor of v_f/v_s at a given distance from the source than the slower beam, a behavior opposite to that predicted for a constant opening angle jet. Third, it is possible that the shaded beam will be colder and, hence, have a smaller Mach angle. Assuming that the jet and counter-jet have the same speed, the shaded side will be denser at a given distance from the source and will therefore be brighter.

For HH 444, in which the faster jet beam has a radial velocity about 2.5 times that of the slower beam, the first model predicts that the slower beam will be about 10 times brighter than the faster beam about the observed brightness asymmetry. With a combination of spectra and images that measure the jet speeds and opening angles, it will be possible to distinguish the dominant mechanism generating other observed irradiated jet asymmetries.

So far, mass-loss rates and other properties have been estimated for only a few irradiated jets (Bally et al. 2000, Bally & Reipurth 2001). These analyses show that the irradiated microjets in the core of the Orion Nebula have very small mass-loss rates, about $\dot{M} \sim 10^{-9}\,M_\odot\ yr^{-1}$, orders of magnitude smaller than that of most other classes of YSO outflow. However, the larger irradiated jets in the outskirts of the Nebula have mass-loss rates that are nearly one order of magnitude larger. Such feeble activity may indicate that the young stars are nearing the ends of their outflow production phase.

8. GIANT HH FLOWS

Until the mid-1990s, the dimensions of HH flows were generally assumed to be around a fraction of a parsec. This view was challenged when Bally & Devine (1994) postulated, on morphological grounds, that a string of HH objects near HH 34 in the L1641 cloud in Orion, hitherto assumed to be separate flows (Reipurth 1989b), is in fact a single giant HH flow with a projected length of about 2.8 pc. This hypothesis was subsequently confirmed by radial velocity and proper motion measurements (Devine et al. 1997), which demonstrate that all HH objects suspected of being part of this parsec-scale flow move away from the HH 34 source. The northern chain of HH objects is redshifted while the southern lobe is blueshifted. Prior to 1994, HH flows of such large dimensions had only been seen in association with newborn luminous stars, such as Z CMa (Poetzel et al. 1989) or the embedded $2 \times 10^4\ L_\odot$ source that powers the 5.3-pc–long HH 80/81 complex (Rodríguez & Reipurth 1989, Martí et al. 1993).

The second parsec-scale HH flow from a low-mass young star to be recognized is associated with HH 1/2, which was initially thought to have a total length of only 0.4 pc. However, Ogura (1995) recognized that two large, bow-shaped emission nebulae, HH 401 and 402, are located symmetrically around the HH 1/2 source, which suggests that they form a giant flow with a projected length of 5.9 pc.

Dozens of parsec-scale HH flows driven by low-mass young stars have been recognized by now (e.g., Bally et al. 1995, 1996b, 1997, Reipurth et al. 1997a, Gómez et al. 1997, Eislöffel & Mundt 1997, Reipurth et al. 1998b, Devine et al. 1999a–c, Bally et al. 1999, Stanke et al. 1999, Wolf-Chase et al. 2000). As an example, Figure 12 shows the giant HH 111 flow complex spanning 7.7 pc. The largest flows detected so far are nearly 12 pc in total extent. Many HH objects not previously recognized to be associated with each other have turned out to trace various parts of single giant outflows. In retrospect, the existence of giant HH flows is not surprising since; for a typical velocity of 100 km s^{-1}, a clump of material much denser than its surroundings can move a parsec in 10^4 years. Thus, ejecta can move more than 10 pc from their sources during the typical 10^5-year duration of protostellar accretion and mass loss.

Giant HH flows provide fossil records of the evolution of protostars and their outflow activity since the flow dynamical ages, typically several times 10^4 years, can approach the accretion ages of their sources.

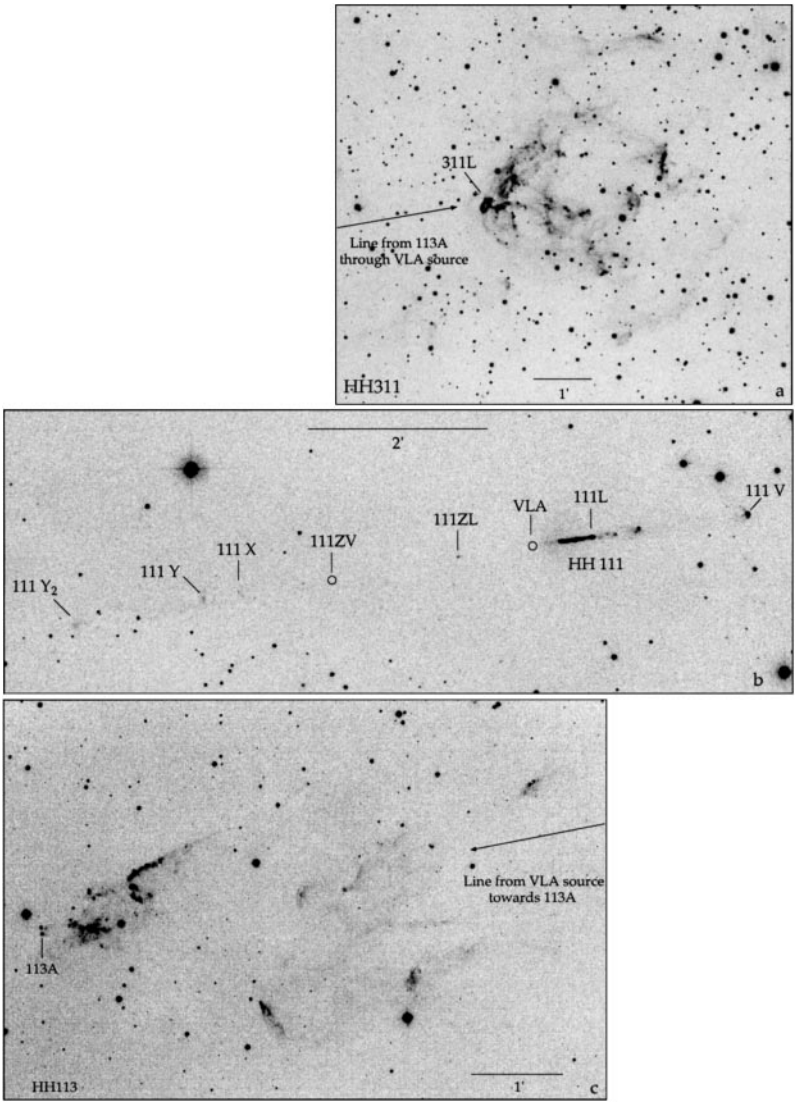

Figure 12 The main components of the 7.7-pc HH 111 giant jet complex. (*Top, bottom panels*) The two terminal working surfaces as seen in Hα + [SII] images from the ESO New Technology Telescope; (*middle panel*) a KPNO 0.9-m [SII] image of the HH 111 jet itself.

8.1. Properties of Giant HH Flows

Parsec-scale flows and their individual HH objects exhibit several systematic trends. Most giant HH flows contain multiple groups of HH objects along their outflow axes, providing evidence for variability in their ejection velocities, ejection directions, and possibly mass-loss rates and degree of collimation. A comparison of the observed proper motions or radial velocities with the shock velocities deduced from the excitation of spectral lines indicates that most HH objects are internal working surfaces formed where previously launched but slower ejecta are overtaken by more recently ejected but faster material (Raga et al. 1990).

8.1.1. SPACING AND MORPHOLOGY OF SHOCKS The spacing of shocks, their sizes, and their morphological complexity tend to increase with increasing distance from the source. Some HH flows contain nearly continuous jets within 0.1 pc of their source. At somewhat larger distances, isolated bow shocks separated by several arcminutes are seen. In many giant flows, large gaps (>10 arcmin) occur between the outermost shocks. Although HH objects near their source tend to consist of compact jets or relatively simple bow shocks, the more distant, and therefore older, HH objects often exhibit complex and chaotic structure consisting of knotty filaments and compact bow shocks embedded in larger bow-shaped or amorphous emission regions. The giant flows associated with HH 1/2, HH 34, and HH 111 illustrate these trends.

8.1.2. KINEMATICS OF INTERNAL SHOCKS There is a systematic decrease in the proper motions and radial velocities of HH objects with increasing distance from the source [cf. HH 34 (Devine et al. 1997), HH 111 (Reipurth et al. 1997a)]. It is possible that the observed velocity field could be the result of a secular increase in the ejection velocity of the jet. However, Cabrit & Raga (2000) find that this would require an unreasonably rapid and relatively recent increase in the jet ejection speed. Instead, they show that the observed decrease of radial velocity and proper motion with increasing distance from the source is best fit by models in which ejecta are decelerated by interactions with the medium into which they are moving.

8.1.3. BLOW-OUT Parsec-scale flows have sizes about an order of magnitude larger than the typical cloud cores from which they originate. Thus, many giant flows have punched completely out of their parent molecular clouds and are injecting mass, energy, and momentum into the surrounding interstellar medium. For example, the northern shock in the T Tauri system, the northeastern shocks in the L1551 IRS5 system, and HH 311, the western terminus in the HH 111 system, all lie along lines of sight devoid of CO emission that contain a rich distribution of background stars and even galaxies (cf. Reipurth et al. 1997a).

8.1.4. SYMMETRIES Many parsec-scale flows exhibit S-shaped point symmetry around their sources. Precession or wandering of the outflow axis can lead to

S-shaped symmetry. Examples include HH 34 and the PV Cep flow. Outflow orientation changes may be produced by an isotropic accretion from turbulent cloud cores or envelopes, or by disk reorientation during periastron passage of a companion star in an eccentric orbit. At least one giant flow [HH 366 in Barnard 5 (Bally et al. 1996b)] has C-shaped symmetry, indicating either flow deflection by a wind or more likely motion of the source through the surrounding cloud.

8.1.5. GIANT OUTFLOWS IN H_2 AND CO Giant outflows can also be recognized in the IR- and millimeter-wavelength tracers. Indeed, some high-velocity CO emission is associated with the majority of giant HH flows, and some parsec-scale outflows were first recognized by the large spatial extents of their CO emission (e.g., Bence et al. 1996). In a few flows, CO emission extends beyond the associated optical emission. The giant HH flow powered by IRS 1 in Barnard 5 (HH 366) coexists with a sheath of CO emission whose structure reflects that of the underlying HH flow (Yu et al. 1999). The strongest CO emission coincides with the brightest HH objects. Additionally, faint bow-shaped regions of CO emission can be found beyond the most distant (from the source) HH objects, indicating eruptions prior to that which produced HH 366.

However, in most giant flows, the optical outflow is an order of magnitude larger than the associated high-velocity CO emission region. For example, in HH 1/2, HH 34, and HH 111, the CO outflows are confined to the inner few arcminutes near the source, whereas the HH objects can be traced from their sources for up to 30, 12, and 25 arcmin, respectively (Chernin & Masson 1995, Cernicharo & Reipurth 1996). Evidently, once the jet or wind emerges from the molecular cloud core into the surrounding (atomic or ionized) medium, it runs out of molecules to entrain, and the formation of molecules in the compressed swept-up layer is too inefficient to produce measurable quantities of CO.

The near-IR lines of H_2 can often be used to trace obscured portions of giant flows. For example, Stanke et al. (1998) have found a chain of H_2 emission line regions extending south from the L1641N cluster in the Orion A molecular cloud. This string of features may trace the redshifted counter-flow associated with one of the giant HH flows emerging toward the north from the L1641 cluster (Reipurth et al. 1998b). Several deeply embedded Class 0/I sources in the L1448 molecular cloud in Perseus power parsec-scale outflows visible in the IR lines of molecular hydrogen (Eislöffel 2000), confirming the suggestion of Bally et al. (1997) that several chains of HH objects in the L1448 region likely trace portions of giant outflows. Wolf-Chase et al. (2000) have found parsec-scale CO counterparts to some of these outflows.

These observations provide support for "unified" outflow models in which a fast, collimated, time-dependent, and bipolar jet and/or wind from a YSO that excites HH objects is also the primary engine that powers the lower velocity lobes traced by CO emission (Raga & Cabrit 1993, Masson & Chernin 1993, 1994, Chernin et al. 1994). In this view, molecular gas is entrained by the jet from the environment, and H_2 emission (and to some extent HH objects) traces

the interaction region where the stellar ejecta transfer momentum to the surrounding medium. If the ambient medium is predominantly atomic, the swept-up gas will not be traceable by molecular emission lines and the HH flow may extend much farther than any associated molecular outflow. However, if the ambient medium is predominantly molecular, an extended molecular outflow may be produced.

8.2. The Utility of Giant HH Flows

The large sizes and high dynamical ages of outflows from young, low-mass stars has a number of important implications.

8.2.1. MASS-LOSS HISTORIES OF YSOs The morphology and kinematics of parsec-scale flows can be used to constrain the mass-loss histories of the source YSOs and to probe the evolution of HH objects. Shocks in parsec-scale outflows trace ejecta that are progressively older with increasing distance from the source. With detailed radial velocity, proper motion, and excitation data, it may be possible to partially reconstruct the mass-ejection history of the source YSO and, by inference, its mass-accretion history. The distribution of shocks (continuous jets, closely spaced low-excitation shocks, and widely spaced ones farther away) implies that flow-velocity variations with low amplitudes occur frequently, whereas large-amplitude variations are relatively rare. The inverse correlation between the amplitude of ejection velocity jumps and their frequency of occurrence may be reminiscent of a $1/f$ process.

Outflow lobe symmetries provide clues about source motion and disk orientation changes that may be the signatures of dynamical interactions in multiple-star systems or clusters. Reipurth (2000) suggests that such interactions may play a fundamental role in the triggering of major mass-loss episodes in multiple YSO systems. Thus, stellar dynamics may be involved in the production of giant flows (see Section 12.4).

8.2.2. PROBING "INVISIBLE" GAS IN OUTFLOW LOBES Giant flows that have blown out of their parent clouds and, where galaxies can be seen in the background, may be observable at X-ray and UV wavelengths. Emission produced by fast shocks or absorption lines originating from various ionization states of many elements may be observable. Shock-excited emission may make a substantial contribution to X-ray and UV backgrounds of the Galaxy and provide a new probe of the star formation environment. For the faster flows, the terminal postshock temperatures can exceed 10^6 K. Since the density in the interclump medium of a giant molecular cloud, or in the interstellar medium that surrounds it, can be as low as 0.1 cm^{-3}, the cooling time for the hot component may approach the dynamical timescales of the flow. Thus, the conditions in the terminal shocks of parsec-scale flows that punch into relatively low-density environments may resemble those found in moderately old supernova remnants, and the same shock diagnostics may be applied.

8.2.3. PROBING THE INTERCLUMP MEDIUM Most of the volume inside giant molecular clouds is filled with voids that do not emit strongly in CO. The nature of this interclump medium (ICM) remains unknown. The terminal working surfaces of giant HH flows can be used to probe the nature of the ICM. Analysis of the shock properties can provide information about the ionization state, density, and other physical characteristics of the ICM. For instance, detection of shock-excited H_2 can be used to infer that the preshock medium is predominantly molecular; the presence of Balmer filaments without measurable forbidden line emission (e.g., where the forbidden lines are significantly more than 20 times fainter than the Hα line) would be an indication that the shock is moving into a neutral atomic medium.

8.2.4. ORIGIN OF TURBULENCE IN MOLECULAR CLOUDS Parsec-scale HH flows may be an important source of turbulence in molecular clouds and the surrounding interstellar medium and may contribute to the self-regulation of star formation. Giant flows sweep up and expel gas from the parent cloud core and inject it into the surrounding ICM and, in cases where the source lies near the edge of a molecular cloud, into the surrounding interstellar medium. The classical high-velocity molecular outflows [v(CO) $>$ 10 km s^{-1} (cf. the L1551 CO outflow)] are likely to be accelerated during the initial stages of this process. By the time an HH flow and its associated molecular outflow reaches parsec dimensions, the velocity of the entrained CO is likely to have declined to very low values and may be hard to distinguish from the surrounding cloud [cf. the CO counterpart to HH 366 in Barnard 5 (Yu et al. 1999) and the RNO 43 giant CO outflow (Bence et al. 1996)]. However, at these late stages, the flow is likely to have produced large cavities in the surrounding cloud. Indeed, some HH flows are seen toward cavities visible in optically thin molecular tracers such as ^{13}CO. The HH 1/2 giant flow is propagating inside a pair of large cavities surrounding the central source. The giant HH 310 outflow is propagating along a large cavity located along the eastern rim of the Orion A cloud (Reipurth et al. 1998b). Other examples of outflow cavities can be seen in L1551 (Snell et al. 1980) and the Circinus cloud (Bally et al. 1999). These cavities indicate that outflows can significantly alter the structure of molecular clouds. Eventually the mass motions degrade through momentum-conserving interactions and start to blend with the surrounding medium. The nonlinear growth of instabilities in radiative shocks and the random orientations of flows will likely make the final state chaotic and turbulent. Many studies have shown that the energy input from outflows can regenerate the observed turbulent motions in molecular clouds on timescales of about 10^6 years (e.g., Bally et al. 1996a).

8.2.5. CHEMICAL REJUVENATION OF MOLECULAR CLOUDS Fast shocks associated with the terminal working surfaces of parsec-scale flows dissociate molecules, resulting in a "chemical rejuvenation" of star-forming molecular clouds. Dissociation of molecules effectively resets the conditions of the affected region to its "initial" chemical state. Therefore, shocks powered by young stars may contribute

to the production of the large abundance of atomic and ionic species, such as C I and C II in the ICM. Thus, these species may not require UV irradiation from O or B stars for their production. Chemical rejuvenation must be an important process in the vicinity of young clusters such as NGC 1333 (Bally et al. 1996a), where dozens of active flows simultaneously churn the surrounding medium and where the mean time between the passage of dissociating shocks over random parcels of gas can be short compared with the evolutionary timescale of the cloud. Thus, outflows may play a basic role in preventing the chemical aging of clouds and in the maintenance of relatively stable and universal molecular abundances.

8.3. The Deflection of HH Flows

With the recognition of the enormous distances traversed by some HH flows, the question arises whether such flows, once escaped from their parent cloud, would coast unimpeded through the ICM. Given the complex structure of molecular clouds, it could be imagined that part of the same cloud, or another cloud, would lie in the path of the flow. Indeed, a few HH flows show evidence for such flow-cloud collisions. The HH 83 jet system is located in a small cloud core outside the western border of the L1641 cloud in Orion (Reipurth 1989b). Its redshifted lobe points toward L1641 and contains only small and weak shocks until after 1.5 pc, when it reaches an adjacent cloud core in L1641. As it rams into the core, the flow lights up in the bright, large HH 84 complex, which is spread out along the side of the cloud core (Reipurth et al. 1997a).

A true deflection of an outflow lobe occurs in the HH 110 flow. This is a bright, rather collimated HH object, which emanates from the side of a small dense cloud in the L1617 region in Orion (Reipurth & Olberg 1991). All attempts to find an energy source along the flow axis have failed. However, a nearby small flow, HH 270, driven by an embedded VLA source (Rodríguez et al. 1998a) points and moves directly toward the apex of HH 110, where it apparently suffers a grazing collision with a small cloud fragment and is strongly shocked and deflected (Reipurth et al. 1996). Such flow-cloud collisions have been studied analytically by Raga & Cantó (1996) and numerically by de Gouveia Dal Pino (1999), both of which can reproduce the main observed properties of the HH 110 flow.

9. PHYSICAL PROPERTIES OF HH JETS

Despite the ease of observing large numbers of emission lines, it is not easy to determine the mechanical parameters of HH flows from their spectra (e.g., Mundt et al. 1987). Since most HH objects trace the cooling layers behind shock waves, the conditions in the emitting regions tend to be far out of equilibrium. Although electron densities in the emitting gas can be readily estimated from the observed line fluxes, notably the ratio of the [SII] 6717 and 6731 lines, the actual hydrogen densities depend on the uncertain and highly variable ionization fractions. By using shock models, Hartigan et al. (1994) show that it is possible to estimate both the

ionization fractions and shock velocities of the line-emitting parts of the flow from various optical line ratios. However, since only the portions of a flow that have recently (within a cooling time) passed through a shock will emit light, it is difficult to relate these density estimates and flow-speed measurements to outflow mass-loss rates. The physical parameters derived from the line ratios tend to be applicable only locally and to a very small fraction of the entire outflow. Alternatively, the mean total density can be derived from the luminosity in a specific line, such as [OI] 6300, to estimate the number of emitting atoms in the aperture. A measure of the flow velocity then gives a mass-loss rate. However, there are two drawbacks. First, the uncertainty in the often considerable extinction, and second, there may be oxygen atoms that do not emit [OI] 6300, either because the temperature is too low to excite electrons to the upper state or because the temperature is too high and the oxygen is ionized.

With these caveats in mind, one can obtain rough mass-loss rate estimates from observations of HH jets such as HH 34 or HH 111. Typical electron densities for HH flows range from $n_e \approx 10$ cm^{-3} for the faintest objects to $>10^5$ cm^{-3} for the brightest, with typical values in the range 10^2–10^3 cm^{-3}. Ionization fractions range from <1% to nearly fully ionized, with typical values around a few percent for most HH flows. Thus, an order-of-magnitude mass-loss rate for a jet is $\dot{M} \approx 2.6 \times 10^{-8} n_3 V_{100} r_{100}^2 / \chi_{0.1}$ ($M_\odot$ year^{-1}), where n_3 is the electron density in the jet in units of 10^3 cm^{-3}, V_{100} is the jet speed in units of 100 km s^{-1}, r_{100} is the jet radius in units of 100 AU, and $\chi_{0.1}$ is the electron fraction in units of 0.1.

The mechanical luminosity of an HH flow is the kinetic energy supplied per second to the flow (ultimately by the source). It is calculated as the total kinetic energy of the flow divided by its dynamic age, and this can be compared with the stellar luminosity $L_\odot$. For the HH 111 jet, Hartigan et al. (1994) find a mechanical luminosity of 1.5 $L_\odot$, or 6% of the luminosity of the source. For HH 34 they find 0.7 $L_\odot$, and for HH 47 it is 4.1 $L_\odot$.

The momentum supply rate (also called the thrust) of an HH flow is the momentum supplied per second to the flow. It is calculated as the total momentum of the flow divided by its dynamic age, which can be compared with the momentum available in radiation ($L_\odot$/c). As an example, Hartigan et al. (1994) derived a momentum supply rate for the HH 34 jet of 4×10^{-5} $M_\odot$ km s^{-1} year^{-1}. Over 10^5 year, this integrates to 4 $M_\odot$ km s^{-1}.

It is a matter of great interest to know whether magnetic fields are present in HH jets. The component of the magnetic field that is important is the one that lies parallel to the surface of the shock. Where magnetic fields are present, the magnetic pressure in the postshock region can inhibit the compression of the gas as it cools,with potential consequences for the observed spectra. Unfortunately, Hartigan et al. (1994) find that for values of a few microgauss to a few hundred microgauss, the emission line ratios obtained from shocks with stronger magnetic fields are almost indistinguishable from lower-velocity shocks without fields. Field strengths have to increase to many milligauss before one can hope to distinguish via line ratios.

Bacciotti et al. (1995) suggest a spectroscopic diagnostic technique, which is model independent and relies on commonly observed forbidden lines to determine the hydrogen density and excitation temperature of HH jets. The principal assumption is that the ionization of O and N is mainly controlled by charge exchange with atomic hydrogen. This appears to be true for O unless the ionization fraction $x_e \sim 1$ and for N unless $x_e > 0.5$. The assumption about charge exchange then defines the relative abundances of the various ions, and since the electron density n_e can be derived from standard methods, then any line ratio becomes a function of the ionization fraction x_e and the excitation temperature T_e. In an x_e vs T_e diagram, curves of different line ratios will then intersect at the given x_e and T_e of an object. For the HH 34 jet, Bacciotti et al. (1995) find $x_e \sim 0.07$ and for HH 111 $x_e \sim 0.11$, factors of 2 or more higher than those based on shock models. The excitation temperatures are fairly constant, between 4500 and 7000 K. Combining x_e and n_e gives the total hydrogen density, which is determined to about 10^4 cm^{-3} for each jet. Further details are given in Bacciotti et al. (1996, 1997, 1999, 2000) and Bacciotti & Eislöffel (1999).

10. JETS, ENTRAINMENT, AND SHOCK CHEMISTRY

10.1. Entrainment and Molecular Outflow Evolution

Herbig-Haro objects are but one manifestation of outflows from young stars. Other tracers already discussed are H_2 and [FeII] emitting shocks (Section 5), centimeter radio continuum jets (Section 6.2), and maser emission (Section 6.4). Observations of millimeter-wavelength transitions of CO and other molecules originally opened up the study of outflows from young stars and are now key tools for understanding outflow activity (e.g., Bally & Lada 1983, Lada 1985, Bachiller 1996, Bachiller & Tafalla 1999). Figure 13 shows a schematic diagram of the most important tracers of outflow activity from young stars. Most of these tracers are excited by shock phenomena where outflowing fluid elements collide with slower ejecta or ambient gas. In this view, HH objects and near-IR emission line objects define regions in an outflow where energy either is being dissipated within internal shocks or is being transferred to the surrounding medium in terminal shocks (e.g., Hartigan et al. 2000a). Since postshock gas cools rapidly, HH objects only trace the current locations of shocks. Dyson (1984) demonstrated that outflows from low-mass protostars accelerate the surrounding medium predominantly in momentum conserving interactions. Thus, the radiative shocks in these flows are best described as isothermal rather than adiabatic.

In contrast to the optical and near-IR emission lines in HH objects, which require temperatures of at least several thousand degrees to excite, the millimeter-wavelength tracers of outflows are collisionally excited at temperatures of only a few kelvins at the densities typically found in molecular clouds or outflow lobes. Therefore, CO emission traces all of the mass entrained by an outflow that contains at least some molecules (Bachiller 1996, Bachiller & Tafalla 1999). Thus,

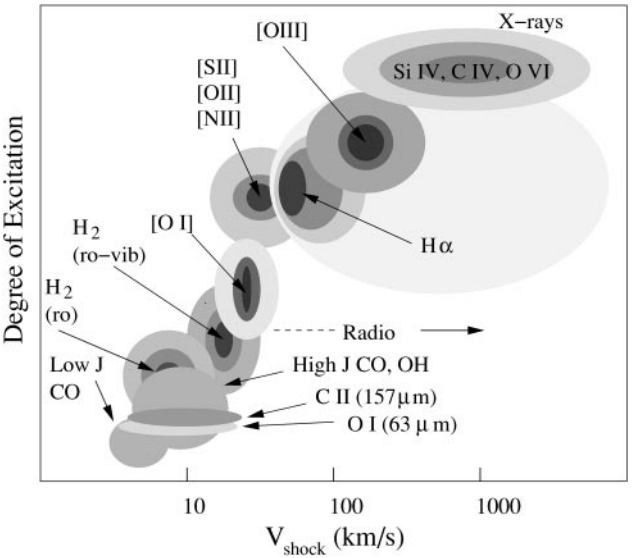

Figure 13 A schematic illustration showing the degree of excitation of the most common emission lines associated with Herbig-Haro objects and stellar outflows as a function of shock velocity. The lower rotational (low-J) states of CO are thermally excited throughout the swept-up gas at the ambient temperature of typical molecular clouds (∼10 K). The radiation from warm (∼50–200 K) postshock gas is dominated by the 63-μm OI and 157-μm CII lines. Emission from molecular gas in postshock layers with temperatures of ∼200–2000 K is dominated by high-J CO and OH emission, and by the pure-rotational and the ro-vibrational states of H_2. The neutral and singly ionized forbidden optical emission lines appear behind faster (>30 km/s) shocks where the 2-eV collisions needed to pump these transitions occur. The near-infrared lines of [Fe II] can be excited by somewhat slower shocks. As shock speeds increase, dissociation, collisional ionization, and ultraviolet shock radiation emitted by the hot plasma immediately behind the shock produce species in successively higher ionization stages. However, the combination of efficient cooling and low recombination rates will usually produce partially ionized plasmas in the postshock cooling layers in which the ionization state is far from thermodynamic balance. Radio continuum emission (both thermal and nonthermal) is sometimes produced behind fast shocks in HH flows.

millimeter-wavelength molecular tracers probe the total mass and momentum deposited into outflow lobes over their lifetimes. Nearly 300 molecular outflows have been discovered so far (e.g., Wu et al. 1996). Though the numbers of CO outflows are comparable to the numbers of HH flows, only about 30% of outflows from young stars are common to both lists. To a large extent this may reflect a variety of selection effects. Although HH objects tend to be visible only from nearby YSOs whose outflow lobes emerge into regions of low obscuration, CO flows can be

detected in both highly embedded and very distant regions, especially when driven by high-luminosity sources.

Molecular outflow lobes can be roughly classified into two types. The "classical" high-velocity CO lobes with $V < 30$ km s^{-1} were first detected in the vicinity of many sources in the early 1980s (Bally & Lada 1983, Lada 1985). These lobes tend to be poorly collimated and contain most of the mass in an outflow. During the 1990s, more sensitive and higher angular resolution maps revealed the presence of highly collimated and extremely high-velocity (EHV) CO components with $V > 30$ km s^{-1} in some outflows. Classical outflow lobes dominate the CO emission associated with mature outflows, whereas EHV components tend to be seen only in the youngest flows (Figure 14). In some systems, the EHV component is resolved

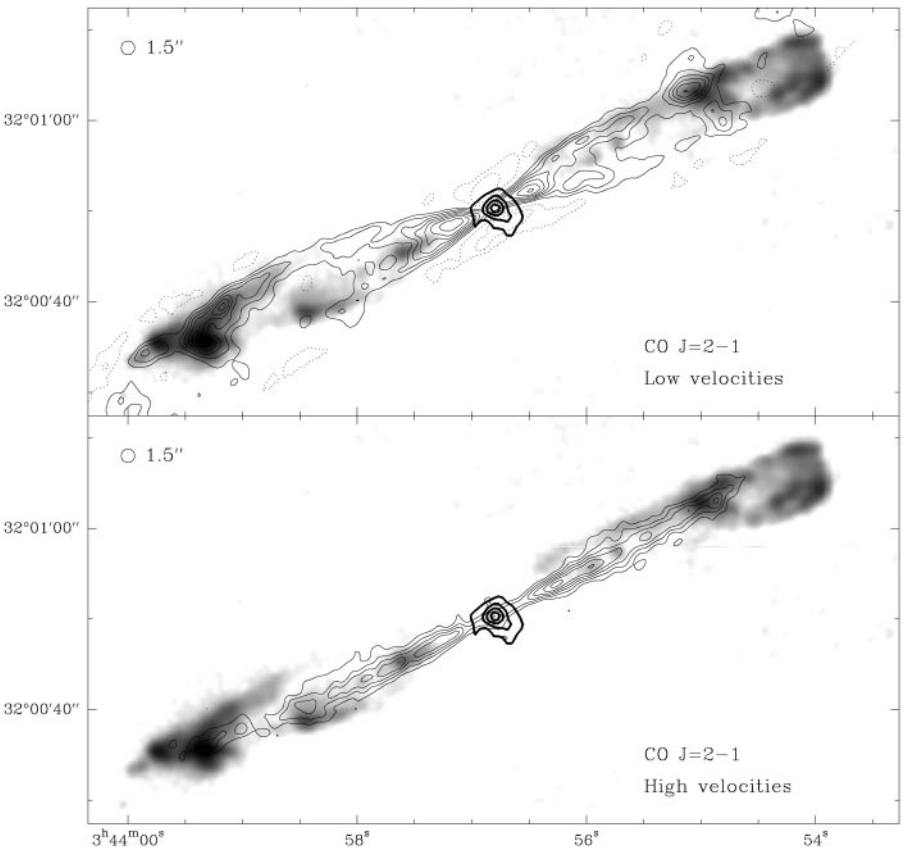

Figure 14 The high-velocity CO ($J = 2 - 1$) outflow surrounding the HH 211 infrared jet. The inner faster flow is more collimated than the outer slower flow. The lobes terminate in infrared molecular hydrogen shocks. The driving source is surrounded by cold dust seen in 1.3-mm continuum emission. [From Gueth & Guilloteau (1999).]

into "molecular bullets," which may trace either high-density molecular jets or the dense gas in the postshock cooling layers where molecule formation may have occurred [e.g., L1448 (Bachiller et al. 1990, Nisini et al. 2000), HH 211 in IC 348 (Gueth & Guilloteau 1999), HH 7–11 (Masson et al. 1990, Bachiller et al. 1998, Koo 1990), HH 111 (Cernicharo & Reipurth 1996, Hatchell et al. 1999)].

There is evidence that the youngest outflow sources preferentially produce high-density molecular jets with $n(H_2) > 10^5\ cm^{-3}$ that have high abundances of various molecules. For example, the L1448C bipolar outflow contains a molecular jet bright in several transitions of SiO that require $n(H_2) > 10^6\ cm^{-3}$ for excitation (Dutrey et al. 1997). The high surface brightness of SiO indicates that the abundance of this molecule has been greatly enhanced by shock processing. Other young sources with SiO jets include SVS 13B in NGC 1333 (Bachiller et al. 1998) and HH 211, which also exhibits a spectacular CO jet (Gueth & Guilloteau 1999). In other extremely young sources, such as L1157, high-density species such as SiO trace knots in the jet or parts of the outflow cavity walls (Gueth et al. 1997). Codella et al. (1999) surveyed protostellar outflows for SiO emission, finding a correlation between SiO emission and source luminosity. For a given luminosity, they found the strongest SiO emission to be associated with the youngest sources.

The best-collimated and highest-density EHV CO jets tend to be associated with highly obscured Class 0 protostars. As a result, their shocks are often best traced by the near-IR emission lines of [FeII] and H_2 but remain invisible in optical tracers. Furthermore, these extremely young outflows tend to have about an order of magnitude larger mechanical-to-bolometric luminosity ratio than the more evolved classical outflow lobes (Bontemps et al. 1996). As the YSOs age and their outflows evolve, the jets carve out large cavities from the surrounding medium to produce the classical outflow lobes. As the extinction decreases, HH objects may become visible within these outflow lobes, but the EHV CO components often become increasingly difficult to detect. Nevertheless, high-velocity CO bullets are seen in several mature outflows, such as HH 111, which have grown to parsec-scale dimensions. As they punch out of their parent clouds, the optical dimensions of these outflows frequently grow to be much larger than the extents of their classical CO outflow lobes [e.g., HH 34 and HH 1/2 (Chernin & Masson 1995), HH 111 (Reipurth et al. 1997a)].

10.2. Jets Vs Wide-Angle Winds

The relationship between molecular outflows and HH objects has been extensively debated during the past two decades (e.g., Cabrit et al. 1997). In unified outflow theories, a primary wind or jet entrains gas from its surroundings by one of several processes (Chernin et al. 1994, Richer et al. 2000). For steady jets, prompt entrainment occurs where fluid elements ram the medium head on, and steady entrainment occurs within the shear layer along the sides of the jet (de Young 1986). Additional types of interaction are possible for time-variable jets. Nonsteady jets with velocity variations produce internal shocks whose debris can splash sideways to widen

the outflow channel, and the collision of the spreading postshock debris with the ambient medium accelerates it (Biro & Raga 1994a,b, Raga & Kofman 1992, Kofman & Raga 1992). When a jet changes its orientation, its terminal working surface will continually interact with new material in different portions of the surrounding cloud to produce many locations where prompt entrainment can occur. Thus, meandering jets can eventually produce very wide outflow cavities. Although masers, radio continuum emission, and shock-excited emission lines trace these interaction regions, molecules such as CO trace the thermal emission produced by the accelerated and entrained postshock gas. These classical CO outflows frequently exhibit shell-like morphologies and have about an order of magnitude lower mean velocity than do HH objects. Thus, highly collimated and time-variable jets can drive poorly collimated lower-velocity molecular outflows by the combined action of jet orientation variations (e.g., precession) and velocity variations, a scenario explored numerically by various groups (e.g., Stone & Norman 1994, Suttner et al. 1997, Smith et al. 1997, Völker et al. 1999).

In an opposing view, a young star produces a wide-angle magnetized wind with a strong radial density dependence, so the emission measure of the optical lines strongly peak toward the axis, giving the appearance of a collimated jet. A significant part ($\sim$0.5) of the mass loss, however, occurs along streamlines with large opening angles. This "collimated wide-angle wind" thus forms a wind-bubble that pushes against the environment. The ambient material is radially swept up by a forward shock, which runs ahead of the wind bubble, and this produces the molecular outflow (e.g., Shu et al. 1991, 1995, 2000, Shang et al. 1998, Matzner & McKee 1999). The precise density and velocity structure of an outflow will depend partly on the structure of the ambient medium, but it will also depend on whether the wide-angle wind is stratified (Li & Shu 1996, Ostriker 1997).

Two types of observations can be used to diagnose the interactions between an outflow and the ambient medium. First, it has been noted that in some CO outflows, the terminal velocities obey a "Hubble law," i.e., the highest-observed radial velocities increase linearly with increasing distance from the source (cf. Shu et al. 1991, Lada & Fich 1996). This behavior can be understood either as a consequence of the sweeping-up of a dense shell from a power law density distribution by a wide-angle wind (Shu et al. 1991) or as the prompt entrainment of ambient material by a bow shock at the head of a jet (Downes & Ray 1999). Second, the decrease of CO line intensity (or mass) with increasing velocity away from the velocity of the host cloud often can be described by either a single power law ($m[v] \propto v^{-\gamma}$) or a broken power law with two distinct slopes (cf. Zhang & Zheng 1997). The steep power-law indices sometimes found at the highest CO outflow velocities have been interpreted as indicating "prompt" entrainment at the head of a jet while the shallower power law indices that frequently characterize the lower velocity "classical" outflow lobes may be associated with "steady state" entrainment. However, Smith et al. (1997) find that the power law describing the line intensity (or mass) as a function of velocity tends to steepen with evolution of the source. Downes & Ray (1999) use numerical models to confirm this result but

find that for nondissociative shocks, entrainment is very inefficient, in that there is relatively little mixing between a jet and the ambient medium.

Despite much effort, observations have so far not resolved the question of whether CO outflows are driven by jets or by wide-angle winds. Some outflows appear to be best explained by one model, whereas others are best fit by the other (e.g., Nagar et al. 1997, Gueth & Guilloteau 1999, Lee et al. 2000).

10.3. Shock Chemistry

Although CO is the most common tracer of outflowing molecular gas, occasionally other species prove to be highly selective tracers of molecular outflows. Molecular abundances can be greatly enhanced behind shocks, in portions of the cloud where shock radiation has penetrated or where ice mantles and grains have been sublimated or sputtered. For example, in the powerful molecular jet associated with HH 197 that is emerging from the Class 0 protostar L1448C in the Perseus cloud, the abundance of SiO is enhanced by a factor of the order of 10^6 with respect to the background cloud (Dutrey et al. 1997). The emission from the high-velocity molecular gas is orders of magnitude brighter than the emission from the background stationary molecular cloud, despite the much smaller column density (Martin-Pintado et al. 1992, Bachiller et al. 1991). The desorption or sputtering of grains in the postshock environment of the jet is the most likely source of such a large abundance enhancement.

Shock processing can alter the gas-phase abundances of dozens of species, such as H_2O, OH, and HCO^+ by up to one or two orders of magnitude (Neufeld & Dalgarno 1989, Hollenbach & McKee1989). Observations show large variations in the abundances of these species from flow to flow and as a function of velocity in a given outflow complex. Recent analyses of abundance variations have been conducted for NGC 1333/IRAS4 and IRAS2 (Blake et al. 1995, Langer et al. 1996, Bachiller et al. 1998), L1641-N (McMullin et al. 1994), HH 25-MMS (Gibb & Davis 1998), BHR-71 (Bourke et al. 1997, Garay et al. 1998), and IRAS16293-2422 (Blake et al. 1994, van Dishoeck et al. 1995). Perhaps the most comprehensive chemical studies have been of the outflow from the Class 0 source in L1157 (Bachiller & Pérez Gutierrez 1997).

Finally, molecular abundances in the stationary gas can also be altered by the radiation fields of passing shocks (Viti & Williams 1999, Taylor & Williams 1996). For example, low velocity or stationary clumps of enhanced HCO^+ emission have been found within several arcseconds of HH objects, including HH 7-11 (Rudolph & Welch 1988), HH 1/2 (Davis et al. 1990), HH 34 (Rudolph & Welch 1992), and HH 80 North (Girart et al. 1998). The coincidence between HH objects and stationary knots of emission in several high dipole moment species has been attributed to radiation-induced abundance variations. Wolfire & Königl (1993) and Viti & Williams (1999) have modeled the time-dependent evolution of the strengths of various millimetric emission lines when strong UV or X-ray radiation fields produced by passing shocks illuminate the surrounding molecular cloud.

11. HH FLOWS FROM MASSIVE STARS

Massive stars also produce powerful outflows during their formation and, where the extinction is not too great, can be seen to excite visible HH objects. There is a general trend that the mechanical luminosity of molecular outflows increases with increasing source luminosity. Thus, the most powerful outflows tend to be associated with the most luminous sources. Although some highly collimated flows are found among these luminous protostars, most outflows from high-mass sources are relatively poorly collimated compared with their lower-mass counterparts. Since high-mass protostars are relatively rare, they tend to be found at much larger distances from us than the low-mass objects. Furthermore, massive protostars tend to be embedded in massive and high-opacity molecular cloud cores. As a result, these flows tend to be obscured, and HH objects are found only rarely in association with massive protostellar outflows.

The nearest massive protostar is embedded in the BN-KL core embedded in the Orion molecular cloud immediately behind the Orion Nebula at a distance of 460 pc. A powerful and massive bipolar molecular outflow emerges from a roughly $10^5\,L_\odot$ protostellar object and is associated with a spectacular set of about a hundred "fingers" of shock-excited H_2 emission (e.g., Allen & Burton 1993, McCaughrean & Mac Low 1997, Tedds et al. 1999, Lee & Burton 2000). Some of these finger tips emerge from the background cloud into the photon dominated region at the interface between the molecular cloud and the Orion Nebula and are associated with the bright HH objects, HH 205 to 210 (Axon & Taylor 1984, O'Dell et al. 1997a). Proper motions indicate a dynamical age of less than 1000 years for the finger system (Jones & Walker 1985, Lee & Burton 2000). The kinetic energy in this outflow, determined from millimeter-wavelength emission lines, is about 10^{48}–10^{49} ergs.

One of the brightest HH objects in the sky, HH 168 (Hartigan et al. 1986), is associated with the $1.7 \times 10^4\,L_\odot$ protostellar source Cepheus A (Sargent 1979). A small cluster of ultracompact HII regions and several powerful H_2O masers are embedded in a region of intense IR emission about 90 arcsec east of HH 168. High-resolution radio continuum observations show that several of these compact HII regions drive arcsecond-scale thermal radio jets. Thus, there are multiple outflows emerging from the Cepheus A star-forming complex, and multiple lobes of high-velocity CO emission have been observed to emerge from this region (e.g., Narayanan & Walker 1996). HH 168 consists of a cluster of high-excitation bow shocks bright in [OIII] and Hα and surrounded by skirts of lower-excitation [SII] emission (Hartigan et al. 2000b). Arcs of 2.122 μm H_2 emission are found both downstream and surrounding the optical features (Hartigan et al. 1996). Hartigan et al. (2000b) found that much of this H_2 emission and some of the [SII] emission is displaced several hundred astronomical units downstream from the shock fronts traced by Hα emission. Thus, the low-excitation lines appear to trace a precursor produced by either shock radiation or a magnetic field.

One of the largest HH outflows powered by a high-luminosity source is associated with the ultracompact HII region G192 in the Gem OB1 association located at

a distance of about 2.2 kpc (Shepherd et al. 1998). This 18-arcmin–long (7 pc) giant HH flow known as HH 396/397 (Devine et al. 1999b) emerges from an opaque cloud core containing a 2×10^4 $L_\odot$ protostar. A nearly continuous chain of knots, filaments, and multiple bow shocks of Hα and [SII] emission extend from within several arcminutes of the source to the ends of the outflow. Although the G192 HH flow is well collimated with a length-to-width ratio greater than 10, there is no evidence for a driving jet.

The objects HH 80/81 in Sagittarius are located at a distance of about 1.7 kpc (Martí et al. 1993). These high-excitation HH objects are bright in [OIII] and exhibit an extremely complex and filamentary structure (Heathcote et al. 1998). They are located at the edge of the host molecular cloud, where a several-parsec–long flow is breaking out into a much-lower–density medium. HH 80/81 exhibit very large radial velocities, with line wings in excess of 700 km s^{-1} and large proper motions with speeds up to 1400 km s^{-1} (Martí et al. 1995, 1998). Furthermore, the HH objects are embedded within a parsec-scale bubble of Hα emission. The jet itself can be traced for several arcminutes from the source toward HH 80/81 by centimeter-wavelength radio continuum observations. Heathcote et al. (1998) note that the cooling distance predicted from the observed line widths and Hα surface brightnesses is several times larger than the size of the objects themselves, which suggests that the heads of the bow shocks should be adiabatic. The emission we see may be either from the bow wings or from a Mach disk. The filamentary structures and huge bow observed downstream from the two bullets may arise if the bullets, upon leaving their cloud environment, suddenly enter a very-low–pressure environment and expand laterally into a Mach cone with a half opening angle $\alpha = \sin^{-1}(3/M_j)$. The observed opening angle indicates a Mach number $M_j \approx 10$, which for a flow velocity of $\sim$650 km s^{-1} corresponds to a sound speed of $\sim$65 km s^{-1}, implying a temperature of $\sim 4.4 \times 10^5$ K. Clearly, HH flows from massive stars open up physical regimes that cannot be explored in flows from low-mass stars.

Although some outflows from high-luminosity sources are collimated, most are not jet driven. Outflows from sources with luminosities of the order of 10^5 $L_\odot$ tend to be very poorly collimated; jet-driven flows such as HH 80/81 tend to have lower luminosities. Although the HH 80/81 complex exhibits the highest velocities of any HH flow, and lower-luminosity sources tend to produce lower flow velocities, there is no clear dependence of flow speed on source luminosity. However, the spatial extents, masses, and mechanical luminosities of outflows do roughly scale with source luminosity.

The acceleration and collimation of outflows from high-luminosity sources may differ from their low-luminosity counterparts in several important respects. Although magnetohydrodynamic processes such as the X-winds (Shu et al. 1994a,b, 1995), Uchida-Shibata bursts (Uchida & Shibata 1985, Shibata & Uchida 1985), or disk winds (Pudritz & Norman 1983, 1986) may dominate the launch of outflows from low-luminosity sources, and magnetic hoop stress and/or ram pressure of accreting envelopes may collimate them into jets (Ostriker 1997), the high-luminosity flows may also derive some of their power from radiation pressure.

Furthermore, ionization and subsequent recombination may contribute to the acceleration of some very large and massive outflows from sources such as Mon R2 (Wolf et al. 1991) and DR21 (Russell et al. 1992). High-mass stars tend to form in clusters. As a result, their outflows may be inflated by the collective effects of many driving sources, or even by a variety of physical processes. Massive stars reach the main sequence rapidly. Thus, during late evolutionary stages, their outflow lobes may continue to be inflated by radiation pressure, expanding HII regions, and even normal stellar winds.

HH flows have also been found associated with a few intermediate-mass Herbig Ae/Be stars, among them MWC 1080 (Poetzel et al. 1992), vBH 65b (Ray & Eislöffel 1994), LkHα 233 (Corcoran & Ray 1998), and HD 163296 (Devine et al. 2000b).

12. THE ENERGY SOURCES OF HH FLOWS

It is a well-established fact that most HH flows are driven by young IR sources embedded in molecular clouds (e.g., Cohen & Schwartz 1983, 1987). In the following, we summarize and discuss the varied properties of HH driving sources.

12.1. Statistical Properties and Evolutionary Stage

The one parameter that can be estimated for all HH sources, embedded and visible, is their luminosity. The two largest compilations of homogeneous HH source luminosities are the ones by Cohen (1990) and Reipurth et al. (1993). Both studies find that the distribution of luminosities is a broad-peaked function with a median value around 11 $L_\odot$. For the most deeply embedded sources, almost all the flux is emitted or reemitted in the IR, principally at far-IR wavelengths (e.g., Cohen & Schwartz 1987). Less-obscured sources can emit a large portion of their luminosity at near-IR wavelengths (e.g., Molinari et al. 1993), where the fluxes occasionally can be highly variable (e.g., Axon et al. 1982). Only few HH sources have so little extinction along the line of sight that they are optically bright stars, the best-known examples being T Tau, DG Tau, HL Tau, RW Aur, and AS 353A, all of which are classical T Tauri stars.

Given that most sources of prominent HH flows are deeply embedded, submillimeter observations have become a very important tool for their study. Generally, very large amounts of circumstellar material are found around these sources, which suggests that as a class, they are among the youngest stars known. Moreover, in many cases, the spectral indices derived indicate that grain growth has already taken place (Reipurth et al. 1993, Dent et al. 1998).

Because of the episodic nature of HH flows, it is difficult to use the flows themselves as an indicator of the evolutionary stage of the underlying source. Beyond classifying the sources as Class 0, I, II, and III, little can be said about the evolutionary stage of individual driving sources. Only for molecular outflows, which to a larger degree represent a time average of outflow activity, has a relation

been established between the outflow momentum flux and the evolutionary stage of the underlying source (Bontemps et al. 1996).

12.2. Eruptive Events

When HH jets are observed to be bipolar, the distribution of blueshifted and redshifted jet knots frequently show near-perfect symmetry, which strongly suggests that knot production is dominated by activity of the central sources and not by interaction with the surrounding medium (Gredel & Reipurth 1994, Zinnecker et al. 1998). Large bow shocks also often show a remarkable symmetry, as in the HH 47, 34, and 355 flows (Graham & Elias 1983, Bührke et al. 1988, Reipurth et al. 1997a). Based on such considerations, it has been suggested that the formation of large HH bow shocks is linked to the FU Orionis (FUor) eruptions (Dopita 1978, Reipurth 1989a). Observationally, FUor eruptions are seen as major brightenings of faint red stars in star-forming regions, leading to F-G type nonemission spectra with low-gravity signatures (Herbig 1966, 1977, 1989, Hartmann & Kenyon 1996). Such eruptions have been successfully modeled as accretion events in circumstellar disks (e.g., Hartmann & Kenyon 1985). It has been suggested that FUor outbursts are triggered either by a runaway instability regulated by the ionization of hydrogen in the inner disk (Bell & Lin 1994, Bell et al. 1995) or by disk perturbations caused by a companion star in a highly eccentric orbit (Bonnell & Bastien 1992, Clarke & Syer 1996).

At the time of this writing, 14 FUors are known. Of these, eight are associated with HH objects. No other class of young stars has anywhere near such a high percentage of association with HH flows. However, most HH sources for which optical and/or IR spectra are available are T Tauri stars. This can be understood by considering the timescales involved. Statistical arguments show that FUor eruptions must be repetitive (Herbig 1977, Hartmann & Kenyon 1985). Although their outburst frequency is at best poorly estimated, it appears that they decay to their low (presumably T Tauri) state on timescales of about a century or more, with large variations for individual objects. The time intervals between the appearance of large working surfaces in HH flows is typically of the order of 500–1000 years. These two timescales imply that an HH energy source at any given time is more likely to be in a lower-accretion T Tauri state than in a higher-accretion FUor state. Obviously, the chance of identifying FUors among HH energy sources should increase with luminosity, as indeed appears to be the case (Reipurth & Aspin 1997). In connection with the above mentioned timescales, it should be mentioned that giant working surfaces may be emitted only during a certain phase in the evolution of the sources, as discussed in Section 12.4.

The luminosities of FUors span a very large range, with the "classical" FUors (FU Ori, V1057 Cyg, V1515 Cyg) reaching many hundreds $L_\odot$. Some of the more recently detected and highly embedded FUors (e.g., L1551 IRS5, HH 354 IRS) have unexpectedly low luminosities around 20 $L_\odot$. The reason behind these differences is not known, and the issue deserves both observational and theoretical examination. One consequence of the existence of low-luminosity FUors is that the

absence of fairly high-luminosity IR sources in many star-forming clouds cannot be taken to imply that such clouds do not harbor FUors. FUors may be more common than currently assumed.

12.3. Binarity

It is well documented that binaries are more common among pre-main sequence stars than among field stars (e.g., Ghez et al. 1993, Reipurth & Zinnecker 1993, Köhler & Leinert 1998), and the driving sources of HH flows are no exception to this. A variety of techniques have been applied to the detection of binarity among HH flow sources. For example, AS353AB, which drives HH 32 (Herbig & Jones 1983), and RW Aur, which drives HH 229 (e.g., Duchene et al. 1999), are visual binaries. IR speckle observations revealed the binarity of Z CMa (Koresko et al. 1991) and T Tauri (Koresko 2000), and NICMOS on board HST has detected a number of close binary HH sources (e.g., Padgett et al. 1999, Reipurth et al. 2000b). Radio continuum interferometry is emerging as a powerful tool for the study of binarity among deeply embedded outflow sources (e.g., Anglada et al. 1992, Rodríguez et al. 1998b, Reipurth et al. 1999).

Reipurth (2000) analyzed a variety of studies of the sources of giant HH flows and found an observed binary frequency between 79% and 86% of which half are higher-order multiples.

12.4. Decaying Triple Systems and Evolution of HH Flows

It is becoming increasingly clear that accretion processes triggered by any disk disturbance will lead to outflow activity. There are a number of mechanisms through which a disk can be disturbed, among these the periastron passage of a binary companion.

Inspired by the extreme multiplicity frequency among giant HH flow sources, Reipurth (2000) has suggested that there may be a causal link between multiplicity and major HH activity. More specifically, it is postulated that the dynamical decay of triple or multiple systems may lead to massive outbursts of outflow. It has long been known that a large fraction of nonhierarchical triple systems break up and eject the lightest member within about a hundred crossing times (e.g., Valtonen & Mikkola 1991, Armitage & Clarke 1997, Sterzik & Durisen 1998), which for typical parameters of multiple stars newly born within a common envelope amounts to several times 10^4 years. At the same time, a closer binary in a highly eccentric orbit is formed. The process of close triple approach will cause serious perturbations and probably direct collisions among the circumstellar disks. Massive disk truncations result, accompanied by large-scale accretion, with a consequent burst of outflow activity. This may be one mechanism that produces giant HH bow shocks. Much of the material culled from the individual circumstellar disks may settle into a circumbinary disk around the newly bound stellar pair. The truncated circumstellar disks can be fed from the circumbinary disk through gas streams, and this as well as other dynamical effects cause the binary orbit to shrink (Artymowicz &

Lubow 1994, 1996). Gas streams together with disk interactions at periastron will drive cyclic accretion modulated on an orbital timescale. As the stellar components gradually spiral toward each other, the increasingly frequent mass-loss events form chains of HH objects, until eventually the binary has a semimajor axis of only 9–12 AU, at which point the closely spaced shocked ejecta appear as a finely collimated jet. In this stellar dynamics jet hypothesis, a jet originates from one (probably the more massive) of the stellar components, and the binary serves to modulate the accretion and thus the outflow on an orbital timescale. The circumstellar and circumbinary disks play different roles: The circumstellar disk interacts with the stellar magnetosphere and provides the jet launch platform despite being truncated to a few astronomical units. The circumbinary disk provides the reservoir of gas for fueling the jet activity. Thus, HH flows formed in this way can be read as a fossil record of the evolution of orbital motions of a binary, newly formed in a triple disintegration event, as it shrinks from a typical separation of 100 AU or more to 10 AU or less. Orbital decay appears to be a very efficient process for such very young binaries and may be completed within a period of the order of 10^4 years. Altogether, the stellar dynamics jet hypothesis suggests that giant HH bow shocks are linked to close triple approaches in a triple or multiple system just prior to breakup and that a highly collimated jet is the result of orbital shrinkage in the resulting binary after the third member has been ejected. Thus, jets witness the brief final phase of dynamical interaction as a close binary is formed, and therefore jets should appear only once from any given binary.

It should, however, be kept in mind that there are many additional ways in which disks, whether around single or binary stars, can become disturbed and lead to outflow activity, possibly resulting in HH jets. Much observational work lies ahead before we have a clearer understanding of how HH jets are formed.

13. UNSOLVED PROBLEMS IN HH RESEARCH

In this article, we have presented an overview of the observations related to HH research as they stand at the end of the year 2000. In the 18 years since the first *Annual Review* article on HH objects was written (Schwartz 1983a), much progress has been made, and we feel confident that certain fundamental aspects of the HH phenomenon have reached a satisfactory explanation. Nonetheless, a number of significant issues have eluded observational efforts so far. We complete this review with a list of what we perceive as the most pressing unsolved problems in HH research today, for many of which current observational techniques do not yet appear adequate.

1. What are the processes that launch and collimate jets, and are these mechanisms a function of the stellar evolutionary stage? Do magnetic fields play a dominant role in these processes?
2. Can we observationally distinguish between models in which jets are single entities, and others where they are integrated with wide-angle winds?

3. What role do stellar companions play in the formation and evolution of jets? How do jets maintain directional stability over long periods of time when most sources are binaries?
4. How do we integrate the many observational facets of jets, such as optical shocks, the presence of molecular hydrogen and possibly dust, thermal and nonthermal radio emission, and the rich molecular shock chemistry? Is there a link between jets and the powerful X-ray emission and flares detected from embedded newborn stars?
5. What are the similarities and differences between jets from young low-mass and high-mass stars? How do protostellar jets relate to the many types of jets and outflows discovered in recent years from various stages of late stellar evolution?

The majority of issues lacking observational data relate to the problem of how HH jets are linked to their driving sources. It will be interesting to see how many of these questions have received a satisfactory answer when the next review on HH flows appears in these pages.

ACKNOWLEDGMENTS

We wish to thank Steve Heathcote for his help and involvement in this review. Jon Morse kindly provided critical comments on the manuscript, and Pat Hartigan and Frederic Gueth permitted us the use of their figures.

LITERATURE CITED

Allen DA, Burton MG. 1993. *Nature* 363:54–56

Anglada G. 1995. *Rev. Mex. Astron. Astrofis. Ser. Conf.* 1:67–76

Anglada G, Rodríguez LF, Cantó J, Estalella R, Torrelles JM. 1992. *Ap. J.* 395:494–500

Anglada G, Villuendas E, Estalella R, Beltrán MT, Rodríguez LF, et al. 1998. *Astron. J.* 116:2953–64

Appenzeller I, Jankovics I, Östreicher R. 1984. *Astron. Astrophys.* 141:108–15

Appl S, Camenzind M. 1993. *Ap. J.* 256:354–70

Armitage PJ, Clarke CJ. 1997. *MNRAS* 285: 540–46

Artymowicz P, Lubow SH. 1994. *Ap. J.* 421: 651–67

Artymowicz P, Lubow SH. 1996. *Ap. J.* 467: L77–80

Aspin C, Sandell G, Russell APG. 1994. *Astron. Astrophys. Suppl.* 106:165–98

Axon DJ, Allen DA, Bailey J, Hough JH, Ward MJ, Jameson RF. 1982. *MNRAS* 200:239–45

Axon DJ, Taylor K. 1984. *MNRAS* 207:241–61

Bacciotti F, Chiuderi C, Oliva E. 1995. *Astron. Astrophys.* 296:185–200

Bacciotti F, Chiuderi C, Pouquet A. 1997. *Ap. J.* 478:594–602

Bacciotti F, Eislöffel J. 1999. *Astron. Astrophys.* 342:717–35

Bacciotti F, Eislöffel J, Ray TP. 1999. *Astron. Astrophys.* 350:917–27

Bacciotti F, Hirth GA, Natta A. 1996. *Astron. Astrophys.* 310:309–14

Bacciotti F, Mundt R, Ray TP, Eislöffel J, Solf J, Camenzind M. 2000. *Ap. J.* 537:L49–52
Bachiller R. 1996. *ARA & A* 34:111–54
Bachiller R, Guilloteau S, Gueth F, Tafalla M, Dutrey A, et al. 1998. *Astron. Astrophys.* 339:L49–52
Bachiller R, Martin-Pintado J, Fuente A. 1991. *Astron. Astrophys.* 243:L21–24
Bachiller R, Martin-Pintado J, Tafalla M, Cernicharo J. Lazareff B. 1990. *Astron. Astrophys.* 231:174–86
Bachiller R, Pérez Gutierrez M. 1997. *Ap. J.* 487:L93–96
Bachiller R, Tafalla M. 1999. See Lada & Kylafis 1999, pp. 227–65
Bally J, Devine D. 1994. *Ap. J.* 428:L65–68
Bally J, Devine D, Alten V. 1996a. *Ap. J.* 473:921–28
Bally J, Devine D, Alten V, Sutherland RS. 1997. *Ap. J.* 478:603–13
Bally J, Devine D, Fesen RA, Lane AP. 1995. *Ap. J.* 454:345–60
Bally J, Devine D, Reipurth B. 1996b. *Ap. J.* 473:L49–53
Bally J, Lada CJ. 1983. *Ap. J.* 265:824–47
Bally J, O'Dell CR, McCaughrean MJ. 2000. *Astron. J.* 119:2919–59
Bally J, Reipurth B. 2001. *Ap. J.* 546:299–323
Bally J, Reipurth B, Lada CJ, Billawala Y. 1999. *Astron. J.* 117:410–28
Bally J, Testi L, Sargent A, Carlstrom J. 1998. *Astron. J.* 116:854–59
Bautista MA, Pradhan AK. 1996. *Astron. Astrophys. Suppl.* 115:551–59
Bautista MA, Pradhan AK. 1998. *Ap. J.* 492: 650–76
Beck-Winchatz B, Böhm KH, Noriega-Crespo A. 1994. *PASP* 106:1271–75
Beck-Winchatz B, Böhm KH, Noriega-Crespo A. 1996. *Astron. J.* 111:346–54
Bell KR, Lin DNC. 1994. *Ap. J.* 427:987–1004
Bell KR, Lin DNC, Hartmann L, Kenyon SJ. 1995. *Ap. J.* 444:376–95
Bence SJ, Richer JS, Padman R. 1996. *MNRAS* 279:866–83
Benedettini M, Giannini T, Nisini B, Tommasi E, Lorenzetti D, et al. 2000. *Astron. Astrophys.* 359:148–58
Bieging JH, Cohen M, Schwartz PR. 1984. *Ap. J.* 282:699–708
Binette L, Cabrit S, Raga AC, Cantó J. 1999. *Astron. Astrophys.* 346:260–66
Biro S, Raga AC. 1994a. *Ap. J.* 434:221–31
Biro S, Raga AC. 1994b. *Astrophys. Space Sci.* 216:127–28
Blake GA, Sandell G, van Dishoeck EF, Groesbeck TD, Mundy LG, Aspin C. 1995. *Ap. J.* 441:689–701
Blake GA, van Dishoeck EF, Jansen DJ, Groesbeck TD, Mundy LG. 1994. *Ap. J.* 428: 680–92
Blandford RD, Payne DG. 1982. *MNRAS* 199: 883–903
Blondin JM, Königl A, Fryxel BA. 1989. *Ap. J.* 337:L37–40
Bonnell I, Bastien P. 1992. *Ap. J.* 401:L31–34
Bontemps S, André P, Terebey S, Cabrit S. 1996. *Astron. Astrophys.* 311:858–72
Bourke TL, Garay G, Lehtinen KK, Koehnenkamp I, Launhardt R, et al. 1997. *Ap. J.* 476: 781–800
Böhm KH. 1956. *Ap. J.* 123:379–91
Böhm KH. 1983. *Rev. Mex. Astron. Astrofis.* 7:55–70
Böhm KH. 1990. In *Structure and Dynamics of the Interstellar Medium*, ed. G Tenorio-Tagle, M Moles, J Melnick, pp. 282–94. Berlin: Springer
Böhm KH. 1995. *Astrophys. Space Sci.* 233:11–25
Böhm KH, Böhm-Vitense E, Brugel EW. 1981. *Ap. J.* 245:L113–17
Böhm KH, Bührke T, Raga AC, Brugel EW, Witt AN, Mundt R. 1987. *Ap. J.* 316:349–59
Böhm KH, Matt S. 2001. *PASP* 113:158–64
Böhm KH, Noriega-Crespo A, Solf J. 1993. *Ap. J.* 416:647–55
Böhm KH, Raga AC, Binette L. 1991. *PASP* 103:85–89
Böhm KH, Schwartz RD, Siegmund WA. 1974. *Ap. J.* 193:353–58
Böhm KH, Solf J. 1990. *Ap. J.* 348:297–311
Böhm-Vitense E, Böhm KH, Cardelli JA, Nemec JM. 1982. *Ap. J.* 262:224–33
Brugel EW, Böhm KH, Böhm-Vitense E, Shull JM. 1985. *Ap. J.* 292:L75–78

Brugel EW, Böhm KH, Mannery E. 1981a. *Ap. J. Suppl.* 47:117–38
Brugel EW, Böhm KH, Mannery E. 1981b. *Ap. J.* 243:874–82
Brugel EW, Shull JM, Seab CG. 1982. *Ap. J.* 262:L35–39
Bührke T, Mundt R, Ray TP. 1988. *Astron. Astrophys.* 200:99–119
Burrows CJ, Stapelfeldt KR, Watson AM, Krist JE, Ballester GE, et al. 1996. *Astron. J.* 473:437–51
Cabrit S, André P. 1991. *Ap. J.* 379:L25–28
Cabrit S, Edwards S, Strom SE, Strom KM. 1990. *Ap. J.* 354:687–700
Cabrit S, Raga AC. 2000. *Astron. Astrophys.* 354:667–73
Cabrit S, Raga AC, Gueth F. 1997. See Reipurth & Bertout 1997, pp. 163–80
Camenzind M. 1990. In *Reviews in Modern Astronomy*, ed., G Klare, 3:234–65. Berlin: Springer
Cantó J, Raga AC, Binette L. 1989. *Rev. Mex. Astron. Astrofis.* 17:65–74
Carr JS. 1993. *Ap. J.* 406:553–62
Ceccarelli C, Haas MR, Hollenbach DJ, Rudolph AL. 1997. *Ap. J.* 476:771–80
Cernicharo J, Lefloch B, Cox P, Cesarsky D, Esteban C, et al. 1998. *Science* 282:462–65
Cernicharo J, Reipurth B. 1996. *Ap. J.* 460: L57–60
Cerqueira AH, de Gouveia Dal Pino EM. 1999. *Ap. J.* 510:828–45
Chernin LM, Masson CR. 1995. *Ap. J.* 443: 181–86
Chernin LM, Masson CR, Dal Pino EM, Benz W. 1994. *Ap. J.* 426:204–14
Chevalier RA, Raymond JC. 1978. *Ap. J.* 225: L27–30
Choe SU, Böhm KH, Solf J. 1985. *Ap. J.* 288: 338–41
Chrysostomou A, Hobson J, Davis CJ, Smith MD, Berndsen A. 2000. *MNRAS* 314:229–40
Clarke CJ, Syer D. 1996. *MNRAS* 278:L23–27
Claussen MJ, Marvel KB, Wootten A, Wilking BA. 1998. *Ap. J.* 507:L79–82
Claussen MJ, Wilking BA, Benson PJ, Wootten A, Myers PC, Terebey S. 1996. *Ap. J. Suppl.* 106:111–32
Codella C, Bachiller R, Reipurth B. 1999. *Astron. Astrophys.* 343:585–98
Cohen M. 1990. *Ap. J.* 354:701–7. Erratum. 1990. *Ap. J.* 362:758
Cohen M, Hollenbach DJ, Haas MR, Erickson EF. 1988. *Ap. J.* 329:863–73
Cohen M, Schwartz RD. 1983. *Ap. J.* 265:877–900
Cohen M, Schwartz RD. 1987. *Ap. J.* 316:311–22
Contopoulos J, Lovelace RVE. 1994. *Ap. J.* 429:139–52
Coppin KEK, Davis CJ, Micono M. 1998. *MNRAS* 301:L10–14
Corcoran M, Ray TP. 1998. *Astron. Astrophys.* 336:535–38
Cox DP, Raymond JC. 1985. *Ap. J.* 298:651–59
Crusius-Wätzel AR. 1990. *Ap. J.* 361:L49–52
Cudworth KM, Herbig GH. 1979. *Astron. J.* 84:548–51
Curiel S, Raga A, Raymond J, Noriega-Crespo A, Cantó J. 1997. *Astron. J.* 114:2736–859
Curiel S, Raymond JC, Wolfire M, Hartigan P, Morse J, et al. 1995. *Ap. J.* 453:322–31
Curiel S, Rodríguez LF, Moran JM, Cantó J. 1993. *Ap. J.* 415:191–203
Davis CJ, Berndsen A, Smith MD, Chrysostomou A, Hobson J. 2000a. *MNRAS* 314:241–55
Davis CJ, Dent WRF, Bell-Burnell SJ. 1990. *MNRAS* 244:173–80
Davis CJ, Eislöffel J, Ray TP. 1994a. *Ap. J.* 426:L93–95
Davis CJ, Mundt R, Eislöffel J. 1994b. *Ap. J.* 437:L55–58
Davis CJ, Mundt R, Eislöffel J, Ray TP. 1995. *Astron. J.* 110:766–75
Davis CJ, Smith MD, Eislöffel J. 2000b. *MNRAS* 318:747–52
de Gouveia Dal Pino EM. 1999. *Ap. J.* 526:862–73
de Gouveia Dal Pino EM, Benz W. 1993. *Ap. J.* 410:686–95
de Gouveia Dal Pino EM, Benz W. 1994. *Ap. J.* 435:261–73

de Gouveia Dal Pino EM, Opher R. 1990. *Rev. Mex. Astron. Astrofis.* 21:477–80
Delamarter G, Frank A, Hartmann L. 2000. *Ap. J.* 530:923–38
Dent WRF, Matthews HE, Ward-Thompson D. 1998. *MNRAS* 301:1049–63
Devine D, Bally J, Reipurth B, Shepherd D, Watson A. 1999a. *Astron. J.* 117:2919–30
Devine D, Bally J, Reipurth B, Stocke J, Morse J. 2000a. *Ap. J.* 540:L57–59
Devine D, Grady CA, Kimble RA, Woodgate B, Bruhweiler FC, et al. 2000b. *Ap. J.* 542:L115–18
Devine D, Reipurth B, Bally J. 1999b. *Astron. J.* 118:972–82
Devine D, Reipurth B, Bally J, Balonek TJ. 1999c. *Astron. J.* 117:2931–40
Devine D, Reipurth B, Bally J, Heathcote S. 1997. *Astron. J.* 114:2095–111
de Young DS. 1986. *Ap. J.* 307:62–72
Dopita MA. 1978. *Ap. J. Suppl.* 37:117–44
Dopita MA, Binette L, Schwartz RD. 1982a. *Ap. J.* 261:183–94
Dopita MA, Schwartz RD, Evans I. 1982b. *Ap. J.* 263:L73–77
Dougados C, Cabrit S, Lavalley C, Ménard F. 2000. *Astron. Astrophys.* 357:L61–64
Downes TP, Ray TP. 1999. *Astron. Astrophys.* 345:977–85
Draine BT. 1980. *Ap. J.* 241:1021–38
Duchene G, Monin JL, Bouvier J, Ménard F. 1999. *Astron. Astrophys.* 351:954–62
Dutrey A, Guilloteau S, Bachiller R. 1997. *Astron. Astrophys.* 325:758–68
Dyson J. 1984. *Astrophys. Space Sci.* 106:181–97
Edwards S, Hartigan P, Ghandour L, Andrulis C. 1994. *Astron. J.* 108:1056–70
Eislöffel J. 2000. *Astron. Astrophys.* 354:236–46
Eislöffel J, Davis CJ, Ray TP, Mundt R. 1994a. *Ap. J.* 422:L91–93
Eislöffel J, Mundt R. 1992. *Astron. Astrophys.* 263:292–300
Eislöffel J, Mundt R. 1994. *Astron. Astrophys.* 284:530–44
Eislöffel J, Mundt R. 1997. *Astron. J.* 114:280–87
Eislöffel J, Mundt R, Böhm KH. 1994b. *Astron. J.* 108:1042–55
Eislöffel J, Mundt R, Ray TP, Rodríguez LF. 2000a. See Mannings et al. 2000, pp. 815–40
Eislöffel J, Smith MD, Davis CJ. 2000b. *Astron. Astrophys.* 359:1147–61
Elias JH. 1980. *Ap. J.* 241:728–35
Everett ME. 1997. *Ap. J.* 478:246–60
Falle SAEG, Innes DE, Wilson MJ. 1987. *MNRAS* 225:741–59
Falle SAEG, Raga AC. 1993. *MNRAS* 261:573–83
Falle SAEG, Raga AC. 1995. *MNRAS* 272:785–99
Fernandes AJL. 2000. *MNRAS* 315:657–68
Fernandes AJL, Brand P. 1995. *MNRAS* 274:639–56
Frank A, Mellema G. 1996. *Ap. J.* 472:684–702
Frank A, Ryu D, Jones TW, Noriega-Crespo A. 1998. *Ap. J.* 494:L79–83
Fridlund CVM, Liseau R. 1994. *Astron. Astrophys.* 292:631–40
Fridlund CVM, Liseau R. 1998. *Ap. J.* 499:L75–77
Garay G, Köhnenkamp I, Bourke TL, Rodríguez LF, Lehtinen KK. 1998. *Ap. J.* 509:768–84
Garnavich PM, Noriega-Crespo A, Raga AC, Böhm KH. 1997. *Ap. J.* 490:752–57
Ghez AM, Neugebauer G, Matthews K. 1993. *Astron. J.* 106:2005–23
Gibb AG, Davis CJ. 1998. *MNRAS* 298:644–56
Girart JM, Estalella R, Ho PTP. 1998. *Ap. J.* 495:L59–62
Gómez M, Kenyon SJ, Whitney BA. 1997. *Astron. J.* 114:265–71
Goodson AP, Böhm KH, Winglee RM. 1999. *Ap. J.* 524:142–58
Goodson AP, Winglee RM. 1999. *Ap. J.* 524:159–68
Goodson AP, Winglee RM, Böhm KH. 1997. *Ap. J.* 489:199–209
Graham JA, Elias JH. 1983. *Ap. J.* 272:615–26
Gredel R. 1994. *Astron. Astrophys.* 292:580–92
Gredel R. 1996. *Astron. Astrophys.* 305:582–91
Gredel R, Reipurth B. 1993. *Ap. J.* 407:L29–32
Gredel R, Reipurth B. 1994. *Astron. Astrophys.* 289:L19–22

Gredel R, Reipurth B, Heathcote S. 1992. *Astron. Astrophys.* 266:439–51
Gueth F, Guilloteau S. 1999. *Astron. Astrophys.* 343:571–84
Gueth F, Guilloteau S, Dutrey A, Bachiller R. 1997. *Astron. Astrophys.* 323:943–52
Hamann F. 1994. *Ap. J. Suppl.* 93:485–518
Hardee PE, Stone JM. 1997. *Ap. J.* 483:121–35
Haro G. 1952. *Ap. J.* 115:572–72
Haro G. 1953. *Ap. J.* 117:73–82
Hartigan P. 1989. *Ap. J.* 339:987–99
Hartigan P, Bally J, Reipurth B, Morse JA. 2000a. See Mannings et al. 2000, pp. 841–66
Hartigan P, Carpenter JM, Dougados C, Skrutskie MF. 1996. *Astron. J.* 111:1278–85
Hartigan P, Curiel S, Raymond J. 1989. *Ap. J.* 347:L31–34
Hartigan P, Edwards S, Ghandour L. 1995. *Ap. J.* 452:736–68
Hartigan P, Lada CJ, Tapia S, Stocke J. 1986. *Astron. J.* 92:1155–61
Hartigan P, Morse J, Bally J. 2000b. *Astron. J.* 120:1436–48
Hartigan P, Morse J, Heathcote S, Cecil G, Raymond J. 1993. *Ap. J.* 414:L119–21
Hartigan P, Morse J, Palunas P, Bally J, Devine D. 2000c. *Astron. J.* 119:1872–80
Hartigan P, Morse J, Raymond J. 1994. *Ap. J.* 436:125–43
Hartigan P, Morse JA, Tumlinson J, Raymond J, Heathcote S. 1999. *Ap. J.* 512:901–15
Hartigan P, Raymond J. 1993. *Ap. J.* 409:705–19
Hartigan P, Raymond J, Hartmann L. 1987. *Ap. J.* 316:323–48
Hartigan P, Raymond J, Meaburn J. 1990. *Ap. J.* 362:624–33
Hartmann L, Kenyon SJ. 1985. *Ap. J.* 299:462–78
Hartmann L, Kenyon SJ. 1996. *Annu. Rev. Astron. Astrophys.* 34:207–40
Hartmann L, Raymond J. 1984. *Ap. J.* 276:560–71
Hartmann L, Raymond JC. 1989. *Ap. J.* 337:903–16
Hatchell J, Fuller GA, Ladd EF. 1999. *Astron. Astrophys.* 346:278–84
Heathcote S, Morse JA, Hartigan P, Reipurth B, Schwartz RD, Bally J, Stone JM. 1996. *Astron. J.* 112:1141–68
Heathcote S, Reipurth B. 1992. *Astron. J.* 104:2193–212
Heathcote S, Reipurth B, Raga A. 1998. *Astron. J.* 116:1940–60
Henney WJ, Raga AC, Axon DJ. 1994. *Ap. J.* 427:305–14
Henriksen RN, Mirabel IF, Ptuskin VS. 1991. *Astron. Astrophys.* 248:221–26
Herbig GH. 1950. *Ap. J.* 111:11–14
Herbig GH. 1951. *Ap. J.* 113:697–99
Herbig GH. 1966. *Vistas Astron.* 8:109–25
Herbig GH. 1969. In *Non-Periodic Phenomena in Variable Stars*, ed. L Detre, pp. 75–84. Dordrecht, Ger.: Reidel
Herbig GH. 1973. *Information Bulletin Variable Stars* No. 832
Herbig GH. 1977. *Ap. J.* 217:693–715
Herbig GH. 1989. See Reipurth 1989c, pp. 233–46
Herbig GH, Jones BF. 1981. *Astron. J.* 86:1232–44
Herbig GH, Jones BF. 1983. *Astron. J.* 88:1040–52
Hester JJ, Stapelfeldt KR, Scowen PA. 1998. *Astron. J.* 116:372–95
Heyvaerts J, Norman CA. 1989. *Ap. J.* 347:1055–81
Hirth GA, Mundt R, Solf J. 1994a. *Astron. Astrophys.* 285:929–42
Hirth GA, Mundt R, Solf J, Ray TP. 1994b. *Ap. J.* 427:L99–102
Hirth GA, Mundt R, Solf J. 1997. *Astron. Astrophys. Suppl.* 126:437–69
Hodapp KW. 1994. *Ap. J. Suppl.* 94:615–49
Hodapp KW. 1999. *Astron. J.* 118:1338–46
Hollenbach D. 1985. *Icarus* 61:36–39
Hollenbach D. 1997. See Reipurth & Bertout 1997, pp. 81–98
Hollenbach D, McKee CF. 1989. *Ap. J.* 342:306–36
Johnstone D, Hollenbach D, Bally J. 1998. *Ap. J.* 499:758–76
Jones BF, Herbig GH. 1982. *Astron. J.* 87:1223–32

Jones BF, Walker MF. 1985. *Astron. J.* 90: 1320–23
Kofman L, Raga AC. 1992. *Ap. J.* 390:359–64
Köhler R, Leinert C. 1998. *Astron. Astrophys.* 331:977–88
Königl A. 1982. *Ap. J.* 261:115–34
Königl A. 1989. *Ap. J.* 342:208–23
Königl A, Pudritz RE. 2000. See Mannings et al. 2000, pp. 759–88
Königl A. Ruden SP. 1993. In *Protostars and Planets III*, ed. EH Levy, JI Lunine, pp. 641–88. Tucson: Univ. Arizona Press
Koo BC. 1990. *Ap. J.* 361:145–49
Koresko CD. 2000. *Ap. J.* 531:L147–49
Koresko CD, Beckwith SVW, Ghez AM, Matthews K, Neugebauer G. 1991. *Astron. J.* 102:2073–78
Krist JE, Stapelfeldt KR, Burrows CJ, Hester JJ, Watson AM, et al. 1999. *Ap. J.* 515:L35–38
Kwan J. 1997. *Ap. J.* 489:284–92
Kwan J, Tademaru E. 1988. *Ap. J.* 332:L41–44
Kwan J, Tademaru E. 1995. *Ap. J.* 454:382–93
Lada CJ. 1985. *Annu. Rev. Astron. Astrophys.* 23:267–317
Lada CJ, Fich M. 1996. *Ap. J.* 459:638–52
Lada CJ, Kylafis ND, eds. 1999. *The Origin of Stars and Planetary Systems*. Dordrecht, Ger.: Kluwer
Lane AP. 1989. See Reipurth 1989c, pp. 331–48
Langer WD, Castets A, Lefloch B. 1996. *Ap. J.* 471:L111–14
Lavalley C, Cabrit S, Dougados C, Ferruit P, Bacon R. 1997. *Astron. Astrophys.* 327:671–80
Lavalley-Fouquet C, Cabrit S, Dougados C. 2000. *Astron. Astrophys.* 356:L41–44
Lee CF, Mundy LG, Reipurth B, Ostriker EC, Stone JM. 2000. *Ap. J.* 542:925–45
Lee J, Burton MG. 2000. *MNRAS* 315:11–20
Lery T, Heyvaerts J, Appl S, Norman CA. 1998. *Astron. Astrophys.* 337:603–24
Li ZY, Shu FH. 1996. *Ap. J.* 468:261–68
Liseau R, Huldtgren M, Fridlund CVM, Cameron M. 1996a. *Astron. Astrophys.* 306: 255–66
Liseau R, Ceccarelli C, Larsson B, Nisini B, White GJ, et al. 1996b. *Astron. Astrophys.* 315:L181–84
Liseau R, Giannini T, Nisini B, Saraceno P, Spinoglio L, et al. 1997. See Reipurth & Bertout 1997, pp. 111–20
Livio M. 1999. *Phys. Rep.* 311:225–45
López R, Riera A, Raga AC, Anglada G, Lopez JA, et al. 1996. *MNRAS* 282:470–76
Lovelace RVE, Newman WI, Romanova MM. 1997. *Ap. J.* 484:628–36
Lovelace RVE, Romanova MM, Contopoulos J. 1993. *Ap. J.* 403:158–63
Mannings V, Boss AP, Russell SS, eds. 2000. *Protostars and Planets IV*. Tucson: Univ. Arizona Press
Martí J. Rodríguez LF, Reipurth B. 1993. *Ap. J.* 416:208–17
Martí J, Rodríguez LF, Reipurth B. 1995. *Ap. J.* 449:184–87
Martí J. Rodríguez LF, Reipurth B. 1998. *Ap. J.* 502:337–41
Martin-Pintado J, Bachiller R, Fuente A. 1992. *Astron. Astrophys.* 254:315–26
Masciadri E, Raga AC. 2001. *Astron. J.* 121: 408–12
Masson CR, Chernin LM. 1993. *Ap. J.* 414: 230–41
Masson CR, Chernin LM. 1994. *Astrophys. Space Sci.* 216:113–17
Masson CR, Mundy LG, Keene J. 1990. *Ap. J.* 357:L25–28
Matzner CD, McKee CF. 1999. *Ap. J.* 526: L109–12
McCaughrean MJ, Mac Low MM. 1997. *Astron. J.* 113:391–400
McKee CF, Hollenbach DI, Seab CG, Tielens AGGM. 1987. *Ap. J.* 318:674–701
McMullin JP, Mundy LG, Blake GA. 1994. *Ap. J.* 437:305–16
Meaburn J, Dyson JE. 1987. *MNRAS* 225:863–72
Mellema G, Frank A. 1997. *MNRAS* 292:795–807
Micono M, Davis CJ, Ray TP, Eislöffel J, Shetrone MD. 1998a. *Ap. J.* 494:L227–30
Micono M, Massaglia S, Bodo G, Rossi P, Ferrari A. 1998b. *Astron. Astrophys.* 333:989–1000

Micono M, Massaglia S, Bodo G, Rossi P, Ferrari A. 1998c. *Astron. Astrophys.* 333:1001–6
Miller JS. 1968. *Ap. J.* 154:L57–59
Molinari S, Ceccarelli C, White GJ, Saraceno P, Nisini B, et al. 1999. *Ap. J.* 521:L71–74
Molinari S, Liseau R, Lorenzetti D. 1993. *Astron. Astrophys. Suppl.* 101:59–85
Molinari S, Noriega-Crespo A, Ceccarelli C, Nisini B, Giannini T, et al. 2000. *Ap. J.* 538:698–709
Molinari S, Noriega-Crespo A, Spinoglio L. 2001. *Ap. J.* 547:292–301
Morse J, Heathcote S, Hartigan P, Cecil G. 1993a. *Astron. J.* 106:1139–55
Morse J, Heathcote S, Cecil G, Hartigan P, Raymond C. 1993b. *Ap. J.* 410:764–76
Morse JA, Hartigan P, Cecil G, Raymond JC, Heathcote S. 1992. *Ap. J.* 399:231–45
Morse JA, Hartigan P, Heathcote S, Raymond JC, Cecil G. 1994. *Ap. J.* 425:738–54
Mouri H, Taniguchi Y. 2000. *Ap. J.* 534:L63–66
Mundt R, Brugel EW, Bührke T. 1987. *Ap. J.* 319:275–303
Mundt R, Bührke T, Fried JW, Neckel T, Sarcander M, Stocke J. 1984. *Astron. Astrophys.* 140:17–23
Mundt R, Fried JW. 1983. *Ap. J.* 274:L83–86
Mundt R, Ray TP, Bührke T, Raga AC, Solf J. 1990a. *Astron. Astrophys.* 232:37–61
Mundt R, Ray TP, Raga AC. 1990b. *Astron. Astrophys.* 252:740–61
Nagar NM, Vogel SN, Stone JM, Ostriker EC. 1997. *Ap. J.* 482:L195–98
Narayanan G, Walker CK. 1996. *Ap. J.* 466: 844–65
Neufeld DA, Dalgarno A. 1989. *Ap. J.* 340:869–93
Neufeld DA, Melnick GJ, Harwit M. 1998. *Ap. J.* 506:L75–78
Nisini B, Benedettini M, Giannini T, Clegg PE, di Giorgio AM, et al. 1999. *Astron. Astrophys.* 343:266–72
Nisini B, Benedettini M, Giannini T, Codella C, Lorenzetti D, et al. 2000. *Astron. Astrophys.* 360:297–310
Nisini B, Lorenzetti D, Cohen M, Ceccarelli C, Giannini T, et al. 1996. *Astron. Astrophys.* 315:L321–24
Noriega-Crespo A, Böhm KH, Raga AC. 1990. *Astron. J.* 99:1918–25
Noriega-Crespo A, Garnavich PM, Curiel S, Raga AC, Ayala S. 1997. *Ap. J.* 486:L55–59
Noriega-Crespo A, Garnavich PM, Molinari S. 1998. *Astron. J.* 116:1388–95
O'Dell CR, Hartigan P, Bally J, Morse JA. 1997a. *Astron. J.* 114:2016–28
O'Dell CR, Hartigan P, Lane WM, Wong SK, Burton MG, et al. 1997b. *Astron. J.* 114:730–33
O'Dell CR, Wen Z, Hu X. 1993. *Ap. J.* 410:696–700
Ogura K. 1995. *Ap. J.* 450:L23–26
Oliva E, Moorwood AFM, Danziger IJ. 1990. *Astron. Astrophys.* 240:453–66
Ortolani S, D'Odorico S. 1980. *Astron. Astrophys.* 83:L8–9
Ostriker E. 1997. *Ap. J.* 486:291–306
Ostriker JP, McKee C. 1988. *Rev. Mod. Phys.* 60:1–68
Ouyed R, Pudritz RE. 1997. *Ap. J.* 484:794–809
Padgett DL, Brandner W, Stapelfeldt KR, Strom SE, Terebey S, Koerner D. 1999. *Astron. J.* 117:1490–504
Pelletier G, Pudritz RE. 1992. *Ap. J.* 394:117–38
Poetzel R, Mundt R, Ray TP. 1989. *Astron. Astrophys.* 224:L13–16
Poetzel R, Mundt R, Ray TP. 1992. *Astron. Astrophys.* 262:229–47
Pravdo SH, Rodríguez LF, Curiel S, Cantó J, Torrelles JM, et al. 1985. *Ap. J.* 293:L35–38
Pudritz RE, Norman CA. 1983. *Ap. J.* 274:677–97
Pudritz RE, Norman CA. 1986. *Ap. J.* 301:571–86
Raga AC, Binette L. 1991. *Rev. Mex. Astron. Astrofis.* 22:265–73
Raga AC, Böhm KH. 1985. *Ap. J. Suppl.* 58: 201–24
Raga AC, Böhm KH. 1986. *Ap. J.* 308:829–35
Raga AC, Böhm KH. 1987. *Ap. J.* 323:193–210
Raga AC, Böhm KH, Cantó J. 1996. *Rev. Mex. Astron. Astrofis.* 32:161–74
Raga AC, Böhm KH, Solf J. 1986. *Astron. J.* 92:119–24

Raga AC, Cabrit S. 1993. *Astron. Astrophys.* 278:267–78
Raga AC, Cantó J. 1989. *Ap. J.* 344:404–12
Raga AC, Cantó J. 1996. *MNRAS* 280:567–71
Raga AC, Cantó J, Binette L, Calvet N. 1990. *Ap. J.* 364:601–10
Raga AC, Cantó J, Calvet N, Rodríguez LF, Torrelles JM. 1993. *Astron. Astrophys.* 276:539–48
Raga AC, Kofman L. 1992. *Ap. J.* 386:222–28
Raga AC, López-Martin L, Binette L, López JA, Cantó J, et al. 2000. *MNRAS* 314:681–88
Raga AC, Mateo M, Böhm KH, Solf J. 1988. *Astron. J.* 95:1783–93
Raga AC, Mundt R, Ray TP. 1991. *Astron. Astrophys.* 252:733–39
Raga AC, Noriega-Crespo A. 1998. *Astron. J.* 116:2943–52
Ray TP, Eislöffel J. 1994. *Astron. Astrophys.* 290:605–8
Ray TP, Mundt R, Dyson JE, Falle SAEG, Raga AC. 1996. *Ap. J.* 468:L103–6
Ray TP, Muxlow TWB, Axon DJ, Brown A, Corcoran D, et al. 1997. *Nature* 385:415–17
Raymond JC. 1979. *Ap. J. Suppl.* 39:1–27
Raymond JC, Blair WP, Long KS. 1997. *Ap. J.* 489:314–18
Raymond JC, Hartigan P, Hartmann L. 1988. *Ap. J.* 326:323–33
Reipurth B. 1989a. *Nature* 340:42–44
Reipurth B. 1989b. *Astron. Astrophys.* 220:249–68
Reipurth B, ed. 1989c. *ESO Workshop on Low Mass Star Formation and Pre-Main Sequence Objects*. ESO, Garching
Reipurth B. 2000. *Astron. J.* 120:3177–91
Reipurth B. 2001. *A General Catalogue of Herbig-Haro Objects*. http://www.casa.colorado.edu/hhcat
Reipurth B, Aspin C. 1997. *Astron. J.* 114:2700–7
Reipurth B, Bally J, Devine D. 1997a. *Astron. J.* 114:2708–35
Reipurth B, Bally J, Fesen R, Devine D. 1998a. *Nature* 396:343–45
Reipurth B, Bally J, Graham JA, Lane AP, Zealey W. 1986. *Astron. Astrophys.* 164:51–66
Reipurth B, Bertout C, eds. 1997. *IAU Symp. No. 182: Herbig-Haro Flows and the Birth of Low Mass Stars*. Dordrecht, Ger.: Kluwer
Reipurth B, Chini R, Krügel E, Kreysa E, Sievers A. 1993. *Astron. Astrophys.* 273:221–38
Reipurth B, Devine D, Bally J. 1998b. *Astron. J.* 116:1396–411
Reipurth B, Hartigan P, Heathcote S, Morse J, Bally J. 1997b. *Astron. J.* 114:757–80
Reipurth B, Heathcote S, Yu KC, Bally J, Rodríguez LF. 2000a. *Ap. J.* 534:317–23
Reipurth B, Olberg M. 1991. *Astron. Astrophys.* 246:535–50
Reipurth B, Raga AC. 1999. See Lada & Kylafis 1999, pp. 267–304
Reipurth B, Raga AC, Heathcote S. 1992. *Ap. J.* 392:145–58
Reipurth B, Raga AC, Heathcote S. 1996. *Astron. Astrophys.* 311:989–96
Reipurth B, Yu KC, Heathcote S, Bally J, Rodríguez LF. 2000b. *Astron. J.* 120:1449–66
Reipurth B, Yu KC, Rodríguez LF, Heathcote S, Bally J. 1999. *Astron. Astrophys.* 352:L86–89
Reipurth B, Zinnecker H. 1993. *Astron. Astrophys.* 278:81–108
Reynolds SP. 1986. *Ap. J.* 304:713–20
Richer JS, Shepherd DS, Cabrit S, Bachiller R, Churchwell E. 2000. See Mannings et al. 2000, pp. 867–96
Rodríguez LF. 1997. See Reipurth & Bertout 1997, pp. 83–92
Rodríguez LF, D'Alessio P, Wilner DJ, Ho PTP, Torrelles JM, et al. 1998b. *Nature* 395:355–57
Rodríguez LF, Delgado-Arellano VG, Gómez Y, Reipurth B, Torrelles JM, et al. 2000. *Astron. J.* 119:882–89
Rodríguez LF, Ho PTP, Torrelles JM, Curiel S, Cantó J. 1990. *Ap. J.* 352:645–53
Rodríguez LF, Reipurth B. 1989. *Rev. Mex. Astron. Astrofis.* 17:59–63
Rodríguez LF, Reipurth B. 1994. *Astron. Astrophys.* 281:882–88
Rodríguez LF, Reipurth B. 1996. *Rev. Mex. Astron. Astrofis.* 32:27–33
Rodríguez LF, Reipurth B. 1998. *Rev. Mex. Astron. Astrofis.* 34:13–19

Rodríguez LF, Reipurth B, Raga AC, Cantó J. 1998a. *Rev. Mex. Astron. Astrofis.* 34:69–72
Rosado M, Esteban C, Lefloch B, Cernicharo J, Garcia RJ. 1999a. *Astron. J.* 118:2962–73
Rosado M, Raga AC, Arias L. 1999b. *Astron. J.* 117:462–68
Rudolph A, Welch WJ. 1988. *Ap. J.* 326:L31–34
Rudolph A, Welch WJ. 1992. *Ap. J.* 395:488–93
Russell APG, Bally J, Padman R, Hills RE. 1992. *Ap. J.* 387:219–28
Sargent AI. 1979. *Ap. J.* 233:163–81
Schwartz RD. 1975. *Ap. J.* 195:631–42
Schwartz RD. 1978. *Ap. J.* 223:891–900
Schwartz RD. 1983a. *Annu. Rev. Astron. Astrophys.* 21:209–37
Schwartz RD. 1983b. *Ap. J.* 268:L37–40
Schwartz RD, Burton MG, Herrmann J. 1997. *Astron. J.* 114:272–79
Schwartz RD, Cohen M, Jones BF, Böhm KH, Raymond JC, et al. 1993. *Astron. J.* 106:740–46
Schwartz RD, Cohen M, Williams PM. 1987. *Ap. J.* 322:403–11
Schwartz RD, Greene TP. 1999. *Astron. J.* 117:456–61
Schwartz RD, Schultz ASB, Cohen M, Williams PM. 1995. *Ap. J.* 446:318–30
Schwartz RD, Williams PM, Cohen M, Jennings DG. 1988. *Ap. J.* 334:L99–102
Shang H, Shu FH, Glassgold AE. 1998. *Ap. J.* 493:L91–94
Shepherd DS, Watson AM, Sargent AI, Churchwell E. 1998. *Ap. J.* 507:861–73
Shibata K, Uchida Y. 1985. *PASJ* 37:31–46
Shu FH, Lizano S, Ruden S, Najita J. 1988. *Ap. J.* 328:L19–23
Shu FH, Najita J, Ostriker EC, Shang H. 1995. *Ap. J.* 455:L155–58
Shu FH, Najita J, Ostriker EC, Wilkin F, Ruden S, Lizano S. 1994a. *Ap. J.* 429:781–96
Shu FH, Najita J, Ruden S, Lizano S. 1994b. *Ap. J.* 429:797–807
Shu FH, Najita JR, Shang H, Li ZH. 2000. See Mannings et al. 2000, pp. 789–814
Shu FH, Ruden SP, Lada CJ, Lizano S. 1991. *Ap. J.* 370:L31–34
Smith MD. 1993. *Ap. J.* 406:520–27
Smith MD. 1994a. *MNRAS* 266:238–46
Smith MD. 1994b. *Astron. Astrophys.* 289:256–60
Smith MD, Suttner G, Yorke HW. 1997. *Astron. Astrophys.* 323:223–30
Snell RL, Loren RB, Plambeck RL. 1980. *Ap. J.* 239:L17–22
Solf J. 1987. *Astron. Astrophys.* 184:322–28
Solf J. 1989. See Reipurth 1989c, pp. 399–406
Solf J. 1997. See Reipurth & Bertout 1997, pp. 63–72
Solf J, Böhm KH. 1993. *Ap. J.* 410:L31–34
Solf J, Böhm KH, Raga AC. 1986. *Ap. J.* 305:795–804
Solf J, Böhm KH, Raga AC. 1988. *Ap. J.* 334:229–51
Stahler SW. 1994. *Ap. J.* 422:616–20
Stanke T, McCaughrean MJ, Zinnecker H. 1998. *Astron. Astrophys.* 332:307–13
Stanke T, McCaughrean MJ, Zinnecker H. 1999. *Astron. Astrophys.* 350:L43–46
Stapelfeldt KR, Beichman CA, Hester JJ, Scoville NZ, Gautier TN. 1991. *Ap. J.* 371:226–36
Sterzik MF, Durisen RH. 1998. *Astron. Astrophys.* 339:95–112
Stone JM, Hardee PE. 2000. *Ap. J.* 540:192–210
Stone JM, Norman ML. 1993. *Ap. J.* 413:198–220
Stone JM, Norman ML. 1994. *Ap. J.* 420:237–46
Stone JM, Xu J, Hardee PE. 1997. *Ap. J.* 483:136–47
Stone JM, Xu J, Mundy LG. 1995. *Nature* 377:315–17
Suttner G, Smith MD, Yorke HW, Zinnecker H. 1997. *Astron. Astrophys.* 318:595–607
Taylor K, Münch G. 1978. *Astron. Astrophys.* 70:359–66
Taylor SD, Williams DA. 1996. *MNRAS* 282:1343–48
Tedds JA, Brand PWJL, Burton MG. 1999. *MNRAS* 307:337–56
Torrelles JM, Gómez JF, Garay G, Rodríguez LF, Curiel S, et al. 1998. *Ap. J.* 509:262–69
Uchida Y, Shibata K. 1985. *PASJ* 37:515–35

Valtonen M, Mikkola S. 1991. *Annu. Rev. Astron. Astrophys.* 29:9–29
van Dishoeck EF, Blake GA, Jansen DJ, Groesbeck TD. 1995. *Ap. J.* 447:760–82
Viti S, Williams DA. 1999. *MNRAS* 310:517–26
Völker R, Smith MD, Suttner G, Yorke HW. 1999. *Astron. Astrophys.* 343:953–65
Walsh JR, Ogura K, Reipurth B. 1992. *MNRAS* 257:110–18
Wilking BA, Schwartz RD, Mundy LD, Schultz ASB. 1990. *Astron. J.* 99:344–52
Wilner DJ, Reid MJ, Menten KM. 1999. *Ap. J.* 513:775–79
Wolf GA, Lada CJ, Bally J. 1991. *Astron. J.* 100:1892–902
Wolf-Chase GA, Barsony M, O'Linger J. 2000. *Astron. J.* 120:1467–78
Wolfire MG, Königl A. 1991. *Ap. J.* 383:205–25
Wolfire MG, Königl A. 1993. *Ap. J.* 415:204–17
Wu Y, Huang M, He J. 1996. *Astron. Astrophys. Suppl.* 115:283–84
Yu KC, Bally J, Devine D. 1997. *Ap. J.* 485:L45–48
Yu KC, Billawala Y, Bally J. 1999. *Astron. J.* 118:2940–61
Yu KC, Billawala Y, Smith MD, Bally J, Butner HM. 2000. *Astron. J.* 120:1974–2006
Yusef-Zadeh F. 1990. *Ap. J.* 361:L19–22
Zhang Q, Zheng X. 1997. *Ap. J.* 474:719–23
Zinnecker H, McCaughrean MJ, Rayner JT. 1998. *Nature* 394:862–65
Zinnecker H, Mundt R, Geballe TR, Zealey WJ. 1989. *Ap. J.* 342:337–44

Figure 1 The bipolar HH 47 complex from observations at the ESO New technology Telescope. (*Red*) [SII] emission; (*green*) Hα; (*blue*) [OIII]. The source is embedded in the dense Bok globule.

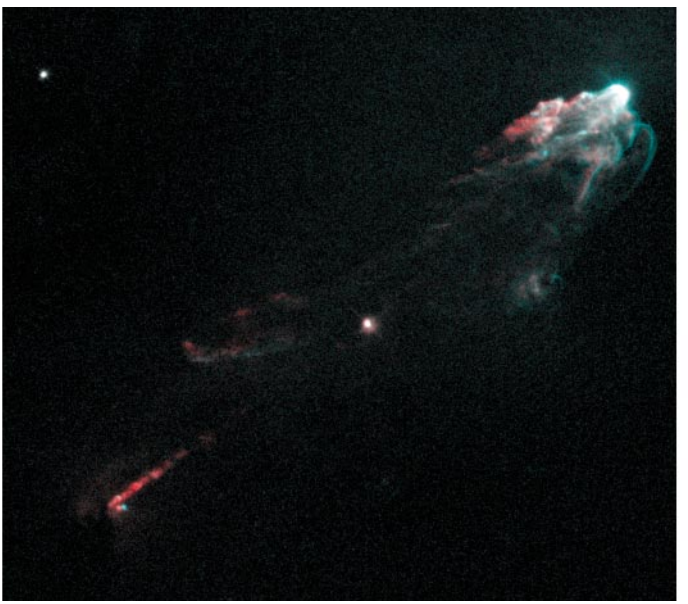

Figure 2 The HH 1 bow shock and jet seen with the Hubble Space Telescope. (*Red*) [SII] emission; (*blue*) Hα.

Figure 3 The L1551 cloud contains several active outflow sources, which together create these chaotic shock structures. Red represents Hα, green [SII]; blue continuum. (*Upper left*) The L1551 IRS5 source; it is associated with a small jet. Images taken at the ESO New Technology Telescope.

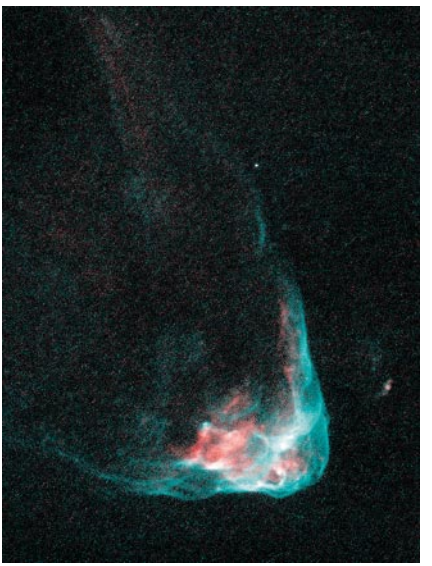

Figure 4 The HH 34 bow shock and Mach disk as seen with the Hubble Space Telescope. The high-excitation bow shock dominates in Hα (*green*) and the low-excitation Mach disk is prominent in [SII] (*red*).

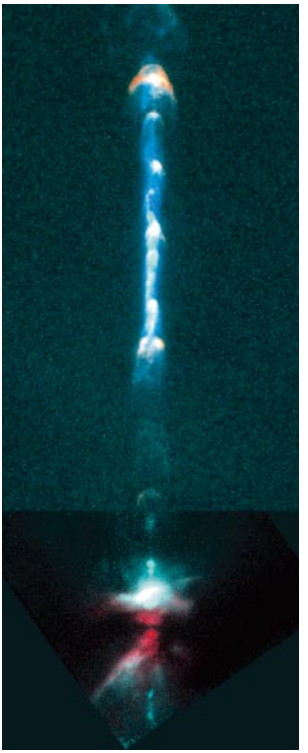

Figure 5 The HH 111 jet and its source region as imaged by the Hubble Space Telescope in the optical and infrared. The main body of the jet is optically visible, whereas the deeply embedded source region is detected only in the infrared.

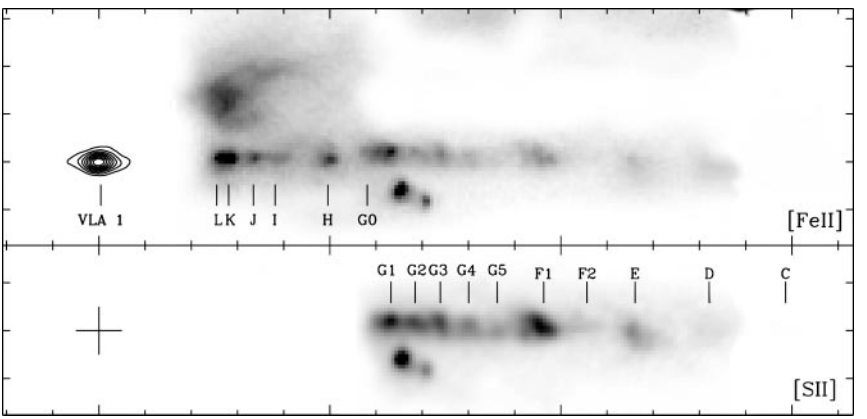

Figure 8 The tiny radio continuum jet around the HH 1 source is seen together with infrared [FeII] and optical [SII] images of the HH 1 jet from the Hubble Space Telescope.

Figure 10 A one-sided, externally irradiated microjet, HH 527, emanates from the proplyd 282–458. The teardrop-shaped ionization front points away from the luminous Trapezium stars in the southern part of the Orion Nebula. No counter jet is visible in this Hubble Space Telescope image even though the extinction appears to be low. (*Black dot*) Location of the young star. The figure spans 8 $\times$ 8 arcsec.

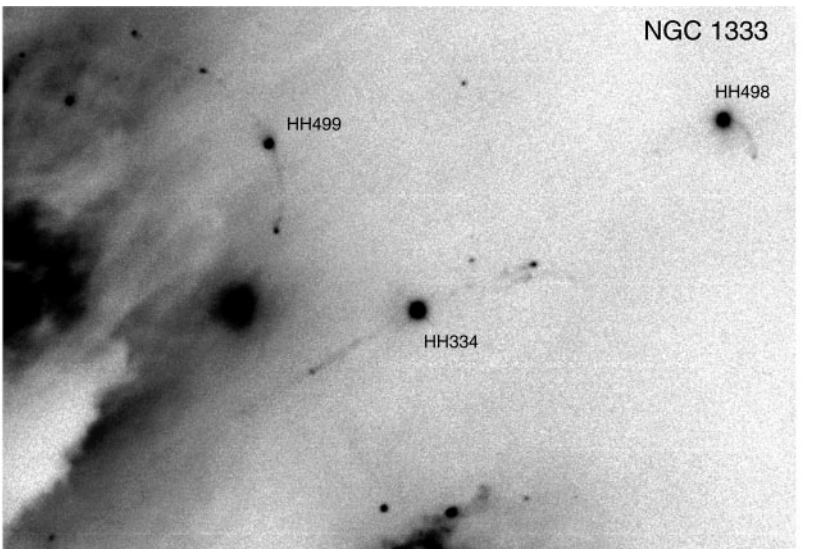

Figure 11 Three irradiated jets associated with visible stars in the NGC 1333 cluster. The bending of the jets is possibly due to the motion of the sources through a stationary medium.

Annual Review of Astronomy and Astrophysics
Volume 39, 2001

CONTENTS